Development of novel tools for dissection of central versus peripheral dopamine D_2-like receptor signaling in dysglycemia

Alessandro Bonifazi[1], Michael Ellenberger[1], Zachary J. Farino[2], Despoina Aslanoglou[2], Rana Rais[3], Sandra Pereira[4,5], José O. Mantilla-Rivas[2], Comfort A. Boateng[1§], Amy J. Eshleman[6,7], Aaron Janowsky[6,7,8], Margaret K. Hahn[4,9,10,11,12], Gary J. Schwartz[13,14], Barbara S. Slusher[3], Amy Hauck Newman[1], Zachary Freyberg[2,15,16*]

[1]Medicinal Chemistry Section, National Institute on Drug Abuse, Intramural Research Program, National Institutes of Health, Baltimore, MD, USA

[2]Department of Psychiatry, University of Pittsburgh, Pittsburgh, PA, USA

[3]Department of Neurology, Johns Hopkins Drug Discovery, The Johns Hopkins University School of Medicine, Baltimore, MD, USA

[4]Centre for Addiction and Mental Health, Toronto, ON, Canada

[5]Department of Physiology, University of Toronto, Toronto, ON, Canada

[6]Research Service, VA Portland Health Care System, Portland, Oregon, USA

[7]Departments of Behavioral Neuroscience and Psychiatry, Oregon Health & Science University, Portland, OR, USA

[8]Methamphetamine Abuse Research Center, Oregon Health & Science University, Portland, OR, USA

[9]Institute of Medical Sciences, University of Toronto, Toronto, ON, Canada

[10]Department of Pharmacology, University of Toronto, Toronto, ON, Canada

[11]Department of Psychiatry, University of Toronto, Toronto, ON, Canada

[12]Banting & Best Diabetes Centre, Toronto, ON, Canada

[13]The Fleischer Institute for Diabetes and Metabolism, Albert Einstein College of Medicine, Bronx, NY, USA

[14]Division of Endocrinology, Department of Medicine, Albert Einstein College of Medicine, Bronx, NY, USA

[15]Department of Cell Biology, University of Pittsburgh, Pittsburgh, PA, USA

[16]Lead Contact

[§]Current affiliation: Department of Basic Pharmaceutical Sciences, High Point University, High Point, NC, USA

[*]Correspondence: freyberg@pitt.edu (Z.F.)

Keywords: Dopamine, dopamine receptors, insulin, diabetes, dysglycemia, pancreas, brain

Abstract

Dopamine (DA) D_2-like receptors in both the central nervous system (CNS) and the periphery are key modulators of metabolism. Moreover, disruption of D_2-like receptor signaling is implicated in dysglycemia. Yet, the respective metabolic contributions of CNS versus peripheral D_2-like receptors including D_2 (D2R) and D_3 (D3R) receptors remain poorly understood. To address this, we developed new pharmacological tools, D_2-like receptor agonists with diminished and delayed blood-brain barrier capability, to selectively manipulate D2R/D3R signaling in the periphery. We designated bromocriptine methiodide (BrMeI), a quaternary methiodide analogue of D2/3R agonist and diabetes drug bromocriptine, as our lead compound based on preservation of D2R/D3R binding and functional efficacy. We then used BrMeI and unmodified bromocriptine to dissect relative contributions of CNS versus peripheral D2R/D3R signaling in treating dysglycemia. Systemic administration of bromocriptine, with unrestricted access to CNS and peripheral targets, significantly improved both insulin sensitivity and glucose tolerance in obese, dysglycemic mice *in vivo*. In contrast, metabolic improvements were attenuated when access to bromocriptine was restricted either to the CNS through intracerebroventricular administration or delayed access to the CNS via BrMeI. Our findings demonstrate that the coordinated actions of both CNS and peripheral D_2-like receptors are required for correcting dysglycemia. Ultimately, the development of a first-generation of drugs designed to selectively target the periphery provides a blueprint for dissecting mechanisms of central versus peripheral DA signaling and paves the way for novel strategies to treat dysglycemia.

Introduction

Dopamine (DA) is increasingly recognized as an important modulator of metabolism[1-13]. Until now, most studies examining dopaminergic modulation of metabolism have primarily focused on DA D_2-like receptors (D_2, D_3 and D_4 receptors) in brain regions associated with metabolic regulation including striatum and hypothalamus[3, 10, 14-16]. For example, hypothalamic dopamine D_2 (D2R) and D_3 (D3R) receptors mediate appetite and feeding behaviors, while blockade of these receptors with antipsychotic drugs (APDs) impairs central glucose sensing[17-22]. Changes in the expression of striatal D_2-like receptors are also associated with overeating and obesity[23, 24]. Moreover, D2R polymorphisms are associated with insulin resistance and type 2 diabetes (T2D)[25]. Nevertheless, the precise mechanisms and sites of action for DA's metabolic effects remain unclear.

Discovery of DA D_2-like receptors outside of the central nervous system (CNS) has expanded the scope of DA's roles as a metabolic modulator[9, 26-28]. In the endocrine pancreas, D2R and D3R are expressed alongside the DA biosynthetic and catabolic machinery in glucagon-secreting α-cells and insulin-secreting β-cells[9, 11, 13, 27, 29, 30]. We and others demonstrated that α- and β-cells produce DA which then acts locally through islet D2R and D3R to negatively modulate hormone secretion in an autocrine/paracrine manner[9, 11, 13, 27, 29, 31, 32]. Importantly, interfering with peripheral D2R/D3R signaling contributes to dysglycemia. We recently discovered that disruption of pancreatic α-cell and β-cell D2R/D3R signaling by APDs significantly elevates insulin and glucagon secretion – hallmarks of dysglycemia[13]. This is consistent with earlier reports of APD-induced hyperinsulinemia and hyperglucagonemia[33-35]. As in T2D, the increases in circulating insulin and glucagon due to disrupted D2R/D3R signaling may desensitize insulin-sensitive peripheral targets (*e.g.*, liver, skeletal muscle, adipose tissue) and stimulate glucose production over time to ultimately produce sustained hyperglycemia and insulin resistance[26, 36, 37]. Conversely, D2R/D3R stimulation with agonists such as bromocriptine or cabergoline acts on

targets in the periphery including pancreatic islets and adipose tissue to improve insulin sensitivity[12, 32, 38-40]. While these drugs can act on other targets (*e.g.*, serotonin and adrenergic receptors), importantly, D2R/D3R agonism appears to be the principal mechanism by which they ameliorate dysglycemia[41]. Indeed, bromocriptine is FDA-approved as a novel therapeutic agent for T2D[42-44]. Taken together, these reports suggest an important role for peripheral D2R/D3R signaling in metabolic regulation and dysglycemia, particularly within the pancreas – observations that have been reproducible across cell, animal, and human studies[26, 28, 37].

To date, it has been difficult to disentangle the respective metabolic contributions of CNS versus peripheral D_2-like receptor signaling to dysglycemia and its effective treatment. Initial work to address the metabolic roles of D_2-like receptors employed transgenic global D2R or D3R knockout (KO) mouse models[10, 15, 45]. However, these D2R or D3R KO mice exhibited complex metabolic phenotypes due to concurrent effects of receptor deletion on both CNS and peripheral targets[15, 45-47]. More recently, mice with constitutive D2R KO specifically in β-cells demonstrated inappropriately elevated serum insulin levels in response to meals, suggesting a key role for β-cell D2R signaling in insulin release *in vivo*[11]. Nevertheless, genetic constitutive KO strategies may still lead to potential compensatory effects at systemic, cellular, and/or transcriptional levels. Such alterations may therefore confound interpretation of metabolic phenotypes, particularly for discerning the relative metabolic contributions of CNS versus peripheral DA signaling.

In lieu of inducible KO models, pharmacological strategies using drugs that selectively stimulate or block DA receptor actions at either CNS or peripheral targets offer an effective alternative approach to dissect central versus peripheral metabolic contributions of DA signaling. Such drug approaches have key advantages since: 1) pharmacological manipulations are reversible, and 2) offer the ability to finely tune changes to receptor signaling either acutely or chronically by

controlling drug doses and durations of exposure. Here, we describe the development of the first generation of new pharmacological tools intended to selectively target peripheral D_2-like receptors. Our aim was to employ peripherally-limited drugs to specifically examine the metabolic relevance of peripheral D_2-like receptor signaling in dysglycemia and its treatment without the confounds of CNS actions. We used quaternary methiodide (MeI) conjugation as a strategy to diminish blood brain barrier (BBB) permeability, selecting bromocriptine methiodide (BrMeI) as our lead compound. We then tested BrMeI *in vivo*, comparing its actions to those of unmodified bromocriptine, to pharmacologically dissect the relative metabolic contributions of CNS versus peripheral D_2-like receptors in dysglycemic mice. Systemic administration of bromocriptine, which has access to both CNS and peripheral targets, significantly improved insulin sensitivity and glucose tolerance. In contrast, selectively limiting D2R/D3R agonism either to the CNS (via intracerebroventricular bromocriptine administration) or to the periphery (via BrMeI) abolished metabolic improvements. Together, these results suggest the importance of coordinated, tandem signaling by both peripheral and CNS D_2-like receptors for glycemic control and offers a new approach both for studying metabolism as well as for the treatment of dysglycemia.

Materials and Methods

Chemistry

General Information. All chemicals and solvents were purchased from the specified chemical suppliers unless otherwise stated and used without further purification. All melting points were determined on an OptiMelt automated melting point system (Stanford Research Systems, Sunnyvale, CA) and were uncorrected. Nuclear magnetic resonance (NMR) spectra including the ^{1}H and ^{13}C NMR spectra were recorded on a Varian Mercury Plus 400 NMR spectrometer (Agilent Technologies, Santa Clara, CA). Proton chemical shifts are reported as parts per million (δ ppm) relative to tetramethylsilane (0.00 ppm) as an internal standard. Coupling constants were

measured in Hz. Chemical shifts for ^{13}C NMR spectra are reported as parts per million (δ ppm) relative to deuterated $CHCl_3$ or deuterated MeOH ($CDCl_3$, 77.5 ppm, CD_3OD 49.3 ppm). Gas chromatography-mass spectrometry (GC/MS) data were acquired (where obtainable) using an Agilent Technologies 6890N GC system equipped with an HP-5MS column (cross-linked 5% PH ME siloxane, 30 m × 0.25 mm i.d. × 0.25 μm film thickness) and a 5973 mass-selective ion detector in electron-impact mode. Ultrapure grade helium was used as the carrier gas at a flow rate of 1.2 mL/min. The injection port and transfer line temperatures were 250°C and 280°C, respectively, and the oven temperature gradient was as follows: the initial temperature (100°C) was held for 3 min, increased to 295°C at 15°C/min over 13 min, and maintained at 295°C for 10 min. All column chromatography was performed using Merck silica gel (230-400 mesh, 60Å; Merck, Rahway, NJ) or via preparative thin layer chromatography using Analtech silica gel (1000 μm; Analtech, Newark, DE). Microanalyses were performed by Atlantic Microlab, Inc. (Norcross, GA) and agree within ±0.4% of calculated values. All compounds were evaluated to be >95% pure based on elemental analysis (see Supplementary Table 1), NMR, HRMS (high resolution mass spectroscopy within ±5 ppm agreement), and MS/MS (ESI in positive mode) approaches.

General procedure for the synthesis of methiodide analogs. A solution of the free base form of the respective parent compounds in acetone or ethanol was added with excess of methyl iodide (3 eq). After 24 h stirring at room temperature in the dark, the solid products were filtered and washed with diethyl ether to yield pure quaternary ammonium salts.

(4a*R*,8a*R*)-5-Methyl-5-propyl-4,4a,5,6,7,8,8a,9-octahydro-2*H*-pyrazolo[3,4-*g*]quinolin-5-ium iodide (AB01-59, (-)-Quinpirole MeI). Commercially available (-)-quinpirole HCl (Tocris, Bristol, United Kingdom; 50 mg, 0.19 mmol) was washed with saturated $NaHCO_3$ aqueous solution and extracted with dichloromethane (DCM). The organic layer was dried with Na_2SO_4, filtered, and

evaporated to yield the free base. The methiodide derivative was prepared according to the general procedure. ^{1}H NMR (400 MHz, CD_3OD) δ 1.05 (t, *J* = 7.2 Hz, 3H), 1.53 (m, 1H), 1.82-1.92 (m, 3H), 2.05-2.15 (m, 2H), 2.43-2.53 (m, 2H), 2.85 (m, 1H), 3.03 (dd, *J* = 4.4, 4.4 Hz, 1H), 3.12 (s, 3H), 3.39-3.70 (m, 6H), 7.46 (br s, 1H). HRMS ESI-MS $[M]^+$ found = 234.1964; calculated = 234.1965. $[\alpha]^{24}_D$ = -65.83° (CH_3OH, *c* = 0.12). m.p. 211-213°C. Anal. ($C_{14}H_{24}IN_3 \cdot 0.5H_2O$) C, H, N. Presence of di-methylated analog ($C_{15}H_{26}IN_3$) observed in HRMS ESI-MS $[M]^+$ found = 248.2118.

(6a*R*,9*R*)-5-Bromo-9-(((2*R*,5*S*,10a*S*,10b*S*)-10b-hydroxy-5-isobutyl-2-isopropyl-3,6-dioxooctahydro-8*H*-oxazolo[3,2-*a*]pyrrolo[2,1-*c*]pyrazin-2-yl)carbamoyl)-7,7-dimethyl-4,6,6a,7,8,9-hexahydroindolo[4,3-*fg*]quinolin-7-ium iodide (AB01-60, Bromocriptine MeI) was prepared according to the general procedure starting from commercially available bromocriptine free base (Santa Cruz Biotechnology, Dallas, TX; 150 mg, 0.23 mmol).^{1}H NMR (400 MHz, CD_3OD) δ 0.75 (d, *J* = 6.4 Hz, 3H), 1.00 (dd, *J* = 6.4, 6.4 Hz, 6H), 1.18 (d, *J* = 6.8 Hz, 3H), 1.75-2.11 (m, 7H), 2.27 (m, 1H), 3.12 (dd, *J* = 12.4, 12 Hz, 1H), 3.30 (br s, 3H), 3.46-3.53 (s and m, 3H and 2H), 3.61 (dd, *J* = 5.6, 6.0 Hz, 1H), 3.80 (dd, *J* = 6.0, 6.0 Hz, 1H), 3.91-4.04 (m, 2H), 4.15-4.19 (m, 1H), 4.49 (dd, *J* = 5.2, 5.6 Hz, 1H), 4.71-4.76 (m, 1H), 6.67 (br s, 1H), 7.16 (t, *J* = 7.8 Hz, 1H), 7.24 (d, *J* = 7.6 Hz, 1H), 7.29 (d, *J* = 7.2 Hz, 1H). ^{13}C NMR (100 MHz, CD_3OD) δ 14.69, 15.83, 20.52, 20.85, 21.51, 21.87, 24.60, 25.80, 33.46, 33.50, 43.33, 45.93, 53.20, 62.64, 64.15, 68.68, 91.17, 104.00, 150.03, 150.60, 110.41, 113.21, 116.29, 122.90, 123.11, 125.20, 130.31, 134.68, 166.04, 166.34, 171.87. HRMS ESI-MS $[M]^+$ found = 668.2449; calculated = 668.2442. $[\alpha]^{24}_D$ = +75.00° (CH_3OH, *c* = 0.32). m.p. 209-210°C. Anal. ($C_{33}H_{43}BrIN_5O_5$) C, H, N.

4-(2,3-Dichlorophenyl)-1-methyl-1-(4-((2-oxo-1,2,3,4-tetrahydroquinolin-7-yl)oxy)butyl)piperazin-1-ium iodide (AB01-61, Aripiprazole MeI) was prepared according to

the general procedure, starting from commercially available aripiprazole free base (Sigma Aldrich, Saint Louis, MO; 50 mg, 0.11 mmol).^{1}H NMR (400 MHz, CD_3OD) δ 1.90-1.93 (m, 2H), 2.05-2.09 (m, 2H), 2.53 (t, *J* = 7.6 Hz, 2H), 2.86 (t, *J* = 7.6 Hz, 2H), 3.26 (s, 3H), 3.44 (m, 4H), 3.62-3.71 (m, 6H), 4.07 (t, *J* = 5.8 Hz, 2H), 6.49 (d, *J* = 2.4 Hz, 1H), 6.59 (dd, *J* = 2.8, 2.4 Hz, 1H), 7.07 (d, *J* = 8.0 Hz, 1H), 7.23-7.32 (m, 3H). m.p. 133°C (decomposition). Anal. ($C_{24}H_{30}Cl_2IN_3O_2$) C, H, N.

7-Hydroxy-*N*-methyl-*N*,*N*-dipropyl-1,2,3,4-tetrahydronaphthalen-2-aminium iodide (AB01-62, 7-OH-DPAT MeI).

Commercially available (±)-7-hydroxy-DPAT HBr (Tocris; 50 mg, 0.15 mmol) was washed with saturated $NaHCO_3$ aqueous solution and extracted with DCM. The organic layer was dried with Na_2SO_4, filtered, and evaporated to yield the free base. The methiodide derivative was prepared according to the general procedure. ^{1}H NMR (400 MHz, CD_3OD) δ 1.04 (t, *J* = 7.0 Hz, 6H), 1.76-1.83 (m, 4H), 1.90-1.95 (m, 1H), 2.40 (m, 1H), 2.82-3.07 (m, 2H), 3.11 (s, 3H), 3.20 (m, 1H), 3.24-3.48 (m, 4H), 3.84 (m, 1H), 6.60 (m, 2H), 6.95 (d, *J* = 8.4 Hz, 1H). m.p. 126-127°C. Anal. ($C_{17}H_{28}INO{\cdot}0.25H_2O$) C, H, N.

(*R*)-*N*,*N*,*N*-Trimethyl-2-oxo-1,2,5,6-tetrahydro-4*H*-imidazo[4,5,1-*ij*]quinolin-5-aminium iodide (MPE01-05, Sumanirole MeI). Sumanirole maleate (230 mg, 1.1 mmol) was synthesized as described previously[48, 49]. The compound was washed with saturated $NaHCO_3$ aqueous solution and extracted with DCM. The organic layer was dried with Na_2SO_4, filtered, and evaporated to yield the free base. The methiodide derivative was prepared according to the general procedure.^{1}H NMR (400 MHz, CD_3OD) δ 3.23 (br s, 9H), 3.36 (m, 1H), 3.82-4.20 (m, 3H), 4.42 (dd, *J* = 2.8, 2.4 Hz, 1H), 6.85-7.15 (m, 3H).^{13}C NMR (100 MHz, CD_3OD) δ 23.86, 24.60, 27.72, 37.62, 40.77, 40.47, 51.93, 68.04, 107.68, 107.80, 113.74, 114.44, 119.51, 119.87, 122.12, 126.25, 126.81, 154.68. ESI-MS $[M]^+$ = 232.11. $[\alpha]^{24}_D$ = -8.33° (CH_3OH, *c* = 0.24). m.p. 180°C (decomposition). Anal. ($C_{13}H_{18}IN_3O{\cdot}H_2O$) C, H, N.

1-((1*H*-Indol-3-yl)methyl)-4-(4-chlorophenyl)-4-hydroxy-1-methylpiperidin-1-ium iodide (MPE01-06, L741,626 MeI) was prepared according to the general procedure, starting from L741,626 free base, prepared as previously described[50] (500 mg, 1.5 mmol).^{1}H NMR (400 MHz, CD_3OD) δ 1.87 (br d, *J* = 14.8 Hz, 2H), 2.42 (td, *J* = 4.0, 2.4, 4.4 Hz, 2H), 3.20 (s, 3H), 3.26-3.31 (m, 2H), 3.43 (dd, *J* = 2.0, 2.0 Hz, 2H), 3.87 (td, *J* = 2.8, 2.8, 2.8 Hz, 2H), 7.17-7.24 (m, 2H), 7.35 (dd, *J* = 2.0, 2.0 Hz, 2H), 7.47-7.59 (m, 3H), 7.70 (s, 1H), 7.80 (d, *J* = 5.6 Hz, 1H). ^{13}C NMR (100 MHz, CD_3OD) δ 32.29, 43.27, 55.15, 63.77, 67.53, 100.71, 110.96, 117.79, 118.04, 118.26, 118.79, 120.48, 121.28, 122.17, 124.48, 126.10, 126.32, 127.82, 128.06, 128.13, 130.09, 132.88, 134.61, 145.21. m.p. 177-178°C. Anal. ($C_{21}H_{24}ClIN_2O$) C, H, N.

(4*S*,4a*R*,10b*R*)-9-Hydroxy-4-methyl-4-propyl-3,4,4a,10b-tetrahydro-2*H*,5*H*-chromeno[4,3-*b*][1,4]oxazin-4-ium iodide (AB01-117, (+)-PD128,607 MeI). Commercially available (+)-PD128,607 HCl (Tocris or OxChem, Wood Dale, IL; 100 mg, 0.15 mmol) was washed with 28% NH_4OH aqueous solution and extracted with DCM. The organic layer was dried with Na_2SO_4, filtered, and evaporated to yield the free base. The methiodide derivative was prepared according to the general procedure.^{1}H NMR (400 MHz, d_6-DMSO) δ 0.91 (t, *J* = 7.2 Hz, 3H), 1.74 (m, 2H), 3.13 (s, 3H), 3.29-3.72 (m, 4H), 3.84 (t, *J* = 9.8 Hz, 1H), 4.02-4.26 (m, 3H), 4.76 (d, *J* = 8.4 Hz, 1H), 5.28 (d, *J* = 9.6 Hz, 1H), 6.61-6.73 (m, 3H), 9.13 (br s, 1H). ^{13}C NMR (100 MHz, CD_3OD) δ 10.92, 15.00, 31.16, 41.18, 59.88, 61.00, 65.83, 66.74, 68.64, 100.55, 100.56 112.30, 117.07, 117.12 121.36, 145.40, 152.14. HRMS ESI-MS $[M]^+$ found = 264.15911; calculated = 264.15942. $[\alpha]^{23}_D$ = +56.8° (CH_3OH, *c* = 0.19). m.p.= 160-162°C. Anal. ($C_{15}H_{22}INO_3 \cdot 1/3NH_4Cl \cdot 1/3H_2O$) C, H, N.

1-Methyl-1-(2-oxo-2-(*m*-tolylamino)ethyl)-4-phenylpiperidin-1-ium iodide (AB01-102, CAB03-015 MeI) was prepared according to the general procedure, starting from CAB03-015

(100 mg, 0.3 mmol) as previously described[51]. ^{1}H NMR (400 MHz, CD_3CN) (mixture of stereoisomers) δ 2.04-2.30 (m, 4H), 2.35 (s, 3H), 2.95 (m, 1H), 3.40 (s, 3H), 3.43 (m, 1H), 3.74-3.88 (m, 2H), 4.03 (br d, *J* = 12.4 Hz, 1H), 4.47 (br s, 2H, isomer 75%), 4.59 (br s, 2H, isomer 25%), 7.03 (d, *J* = 6.4 Hz, 1H), 7.28-7.58 (m, 8H), 9.66 (br s, 1H, isomer 75%), 9.83 (br s, 1H, isomer 25%). ^{13}C NMR (100 MHz, CD_3CN) δ 20.55, 26.81, 27.18, 38.68, 39.06, 45.72, 54.02, 57.38, 62.03, 62.82, 65.27, 67.09, 99.90, 120.58, 122.06, 125.70, 125.76, 126.75, 126.96, 127.27, 128.59, 128.69, 128.77, 128.80, 133.36, 137.58, 138.92, 143.17, 143.27, 161.11. m.p. 57-58°C. Anal. ($C_{21}H_{27}IN_2O$) C, H, N.

Radioligand binding studies

Cell culture and sample preparation. HEK293 cells stably expressing human D2R, D3R, or D4R were grown in a 50:50 mix of DMEM and Ham's F12 culture media supplemented with 20 mM HEPES, 2 mM L-glutamine, 0.1 mM non-essential amino acids, 1x antibiotic/antimycotic, 10% heat-inactivated fetal bovine serum (FBS), and 200 µg/ml hygromycin (Life Technologies, Grand Island, NY) (37°C, 5% CO_2). Upon reaching 80-90% confluence, cells were harvested using pre-mixed Earle's Balanced Salt Solution (EBSS) with 5 mM EDTA (Life Technologies) and centrifuged at 3000 rpm (10 min, 21°C). Following removal of the supernatant, cell pellets were resuspended in 10 mL hypotonic lysis buffer (5 mM $MgCl_2$, 5 mM Tris, pH 7.4 at 4°C) and centrifuged at 20000 rpm (30 min, 4°C). Pellets were subsequently resuspended in fresh binding buffer, with protein concentrations determined via Bradford protein assays (Bio-Rad, Hercules, CA).

Radioligand competition binding. The radioligand [^{3}H]-(R)-(+)-7-OH-DPAT was employed in all competition binding studies with the exceptions of L741,626 and its MeI analogue, MPE01-06, which instead used [^{3}H]-*N*-methylspiperone. For [^{3}H]-(R)-(+)-7-OH-DPAT binding studies, membranes were harvested fresh; the binding buffer was made from 50 mM Tris, 10 mM $MgCl_2$,

1 mM EDTA, pH 7.4. On test day, all test compounds were freshly dissolved in 30% DMSO and 70% H_2O to a stock concentration of 1 mM or 100 µM. For [^{3}H]-*N*-methylspiperone binding studies, the binding buffer was composed of 8.7 g/L Earle's Balanced Salts without phenol red (US Biological, Salem, MA), 2.2 g/L sodium bicarbonate, pH 7.4; 500 µg/ml membranes were stored at -80°C until use. To assist in the solubilization of free-base compounds, 10 µL of glacial acetic acid was added along with DMSO. Each test compound was serially diluted using 30% DMSO vehicle. Membranes were diluted in fresh binding buffer. Radioligand competition experiments were conducted in 96-well plates containing 300 µL fresh binding buffer, 50 µL of diluted test compound, 100 µL of membranes ([^{3}H]-*N*-methylspiperone: 20 µg total protein for hD2R or hD3R; [^{3}H]-(R)-(+)-7-OH-DPAT: 80 µg, 40 µg and 60 µg total protein for hD2R, hD3R or hD4R respectively), and 50 µl of radioligand diluted in binding buffer ([^{3}H]-*N*-methylspiperone: 0.4 nM final concentration, Perkin Elmer, Waltham, MA; [^{3}H]-(R)-(+)-7-OH-DPAT: 1.5 nM final concentration for hD2R, 0.5 nM final concentration for hD3R and 3 nM final concentration for hD4R; ARC, Saint Louis, MO). Nonspecific binding was determined using 10 µM (+)-butaclamol (Sigma-Aldrich) and total binding was determined with 30% DMSO vehicle. All compound dilutions were tested in duplicate or triplicate with reactions incubated at room temperature for either 60 min in [^{3}H]-*N*-methylspiperone studies or for 90 min in [^{3}H]-(R)-(+)-7-OH-DPAT studies. Reactions were terminated by filtration through a Perkin Elmer Uni-Filter-96 GF/B 96-well microplate presoaked in 0.5% polyethylenimine using a Brandel 96-Well Plate Harvester Manifold (Brandel Instruments, Gaithersburg, MD). The filters were washed 3 × 1 mL/well of ice-cold binding buffer. Perkin Elmer MicroScint 20 Scintillation Cocktail (65 µL/well) was added and filters were counted using a Perkin Elmer MicroBeta Microplate Counter. IC_{50} values for each compound were determined from dose-response curves, enabling calculation of K_i values using the Cheng-Prusoff equation[52]. Analyses of receptor binding data were performed using GraphPad Prism (version 6.0; GraphPad Software, San Diego, CA). K_i values for each compound were determined

from at least three independent experiments performed in triplicate. Receptor binding data for (-)-quinpirole and sumanirole parent compounds were previously reported[49].

Mitogenesis assays

DA D_2-like receptor-mediated mitogenesis functional assays were conducted as reported earlier[48, 53]. Briefly, Chinese hamster ovary (CHO) cells expressing human D2R or D3R (CHOp-D2R or CHOp-D3R, respectively) were maintained in α-MEM culture media supplemented with 10% FBS, 0.05% penicillin/streptomycin, and 400 µg/mL geneticin (G418) (37°C, 5% CO_2). To measure D_2-like receptor-mediated stimulation of mitogenesis via D2R or D3R, the respective cell lines were seeded into 96-well plates at a concentration of 5000 cells/well. After 48-72 h, cells were rinsed twice with serum-free α-MEM and incubated for an additional 24 h (37°C, 5% CO_2). On test day, serial dilutions of the test compounds were made in serum-free α-MEM media. Medium was then replaced with 100 µL of the respective test compound dilutions. Following ~24 h of drug incubation (37°C, 5% CO_2), 0.25 µCi of [^{3}H]thymidine in α-MEM supplemented with 10% FBS was added to each well and incubated for an additional 2 h (37°C, 5% CO_2). At the assay conclusion, cells were trypsinized (1% trypsin in Ca^{2+}/Mg^{2+}-free PBS). Plates were then filtered, and intracellular radioactivity was measured via scintillation spectrometry. The D2R/D3R agonist (-)-quinipirole was run each day as an internal control. Specific [^{3}H]thymidine incorporation at each drug dose was expressed as % maximal quinpirole effect for each of the tested drugs. EC_{50} values and E_{max} values for each compound were determined from dose-response curves via nonlinear regression analyses using GraphPad Prism software.

Dopamine D_4 receptor-mediated adenylate cyclase activity/cAMP functional assay

HEK-D4.4-AC1 cells expressing human DA D4.4 receptors and adenylate cyclase type I were used. Experiments were conducted with a cAMP enzyme immunoassay (EIA) kit (Cayman, Ann

Arbor, MI, USA) as described previously[54]. Basal cAMP was subtracted from all cAMP values. Maximal DA D4.4 receptor-mediated inhibition of forskolin-stimulated cAMP formation by the agonist drugs was defined with 1 µM (-)-quinpirole. The maximal effect of the assayed drugs was then normalized to maximal effect of (-)-quinpirole.

Glucose-stimulated insulin secretion assay

Cell culture. INS-1E cells (gift of Dr. Pierre Maechler, Université de Geneve) were cultured as described earlier[11, 27, 55]. Cells were maintained in RPMI 1640 medium supplemented with 5% heat-inactivated FBS, 2 mM L-glutamine, 10 mM HEPES, 1 mM sodium pyruvate, 100 U/mL penicillin/streptomycin, and 50 µM 2-mercaptoethanol (37°C, 5% CO_2).

Glucose-stimulated insulin secretion (GSIS). Assays measuring GSIS in INS-1E cells were conducted as reported earlier[11, 56]. Briefly, INS-1E cells were seeded into a 24-well plate at an initial seeding density of 5.0×10^5 cells/well. RPMI 1640 media was exchanged 24 h following plating and experiments were conducted the next day. On the experimental day, cells were glucose-starved (1 h, 37°C) in KRB and subsequently stimulated with 20 mM glucose in the presence of drugs (90 min, 37°C). At assay conclusion, supernatants were collected for insulin detection.

Insulin measurement and analysis. Secreted insulin was detected using a commercially available insulin detection kit (PerkinElmer/Cisbio Bioassays, Bedford, MA) based on homogenous time-resolved fluorescence resonance energy transfer (HTRF) technology as described previously[11, 56, 57]. Samples were incubated with the antibodies for 2 h at room temperature and then read using a PheraStar FS multi-mode plate reader (BMG Labtech, Ortenberg, Germany). Insulin concentrations (in ng/mL) were derived via extrapolation of ratiometric fluorescence readings (665 nm/620 nm) to a second-order quadratic polynomial curve. Dose-response curves were fit via non-linear regression of Log[drug] versus normalized %

maximum insulin secretion via GraphPad software (version 6.0). IC_{50} and E_{max} values were calculated from the non-linear regression analyses.

NanoBRET

DNA constructs. NanoBRET experiments employed human D2R (DRD2) cDNA tagged at the N-terminus with an IL6 signal sequence followed by a HiBiT tag and tagged at the C-terminus with a HaloTag: IL6-HiBiT-D2R-HaloTag. G protein recruitment studies employed human $G\alpha_{i1}$ with nanoluciferase (NanoLuc) inserted at position 91: NanoLuc-$G\alpha_{i1(91)}$. β-arrestin2 recruitment assays used human β-arrestin2 (ARRB2) fused to NanoLuc at its N-terminus: NanoLuc-β-arrestin2. All constructs were prepared by Genscript USA (Piscataway, NJ) and cloned into a pcDNA3.1(+) vector backbone (Thermo Fisher Scientific, Waltham, MA). Constructs were confirmed by sequencing analysis.

Transfection. HEK-293T cells were transfected after reaching 70% confluency via Lipofectamine 3000 (Thermo Fisher Scientific) (2.5 µg total cDNA) per manufacturer instructions. We used a 100 (IL6-HiBiT-D2R-HaloTag):1 (NanoLuc-$G\alpha_{i1(91)}$ or NanoLuc-β-arrestin2) nanoBRET donor/acceptor pair ratio. Empty pcDNA3.1(+) vector was used to maintain a constant amount of total transfected DNA.

NanoBRET. NanoBRET assays were conducted as described previously[12]. After transfection, cells were plated onto white poly-D-Lysine pre-coated, 96-well, flat bottom plates (Greiner Bio-One, Monroe, NC) at a density of 5×10^4 cells/well. After adhering to the plates overnight, cells were washed with HBSS and labeled with 100 nM HaloTag NanoBRET 618 ligand (Promega Corp., Fitchburg, WI) in phenol red-free Opti-MEM I reduced serum medium (Gibco/Thermo Fisher Scientific) (2 h, 37°C). Cells were washed with HBSS and 5 mM furimazine was added to each well followed by treatment with the respective drugs. Plates were read within 5-10 min after drug addition on a PHERAstar FSX plate reader (BMG Labtech). The nanoBRET ratio was

calculated as the emission of the acceptor (618 nm) divided by the emission of the donor (460 nm). Net nanoBRET values were obtained by subtracting the background nanoBRET ratio from cells expressing only NanoLuc. Data were normalized to the % maximum DA response. NanoBRET data were further normalized to define the minimum and maximum response to the corresponding endogenous ligand. EC_{50} values were calculated by non-linear regression analysis via GraphPad software.

Initial Screening: Receptor and biogenic amine transporter binding assays

General. Test drug BrMeI was weighed and dissolved in DMSO to make a 10 mM stock solution. An initial dilution to 50 µM for binding was made with water (for biogenic amine transporter and DA receptor binding assays) or buffer (for serotonin and opioid receptor binding assays). Subsequent dilutions were made with assay buffer, maintaining a final 0.1% DMSO concentration. Assays for specific binding to D1R, D4R, 5-HT_{1A}, 5-HT_{2A}, and 5-HT_{2C} were performed as previously described[53].

Data analysis. Excel software (Microsoft Inc., Redmond, WA) was used to analyze data. Binding data were normalized to % inhibition of specific control binding. Nonspecific binding was subtracted from all data. Specific binding in the presence of drug was normalized to binding in the absence of drug (control binding).

Dopamine receptor binding assays

***[^{3}H]SCH-23390 D1R binding assay*.** Mouse fibroblast cells expressing human D1R at high density (LhD1 cells) were used. Cells were grown to confluence in DMEM containing 10% FetalClone1 serum (FCS; HyClone, Logan, UT), 0.05% penicillin/streptomycin, and 400 µg/mL G418. One confluent 150 mm plate yielded sufficient membranes for 96 wells with ~10-15 µg protein/well. Cells were collected via scraping and centrifuged at 500 x *g* for 5 min. The pellet was

overlaid with 2 mL assay buffer (50 mM Tris-HCl, 120 mM NaCl, 5 mM KCl, 2 mM $CaCl_2$, 1 mM $MgCl_2$) and stored at -70°C until use. On the experimental day, the pellet was homogenized in assay buffer with a polytron. Cell homogenate (100 µL) was added to wells containing 800 µL of BrMeI or buffer. After 10 min preincubation, 100 µL of [^{3}H]SCH-23390 radioligand (0.18 nM final concentration) was added and incubated at 25°C for 60 min. Reactions were terminated by filtration using a Tomtec 96-well harvester (Tomtec, Hamden, CT) and filter radioactivity was counted using a Perkin Elmer MicroBeta scintillation counter. Nonspecific binding was determined with 1 µM SCH-23390.

[^{3}H]YM-09151-2 D2R and D3R binding assays. CHO cells expressing human D2R or D3R receptor (CHOp-D2 or CHOp-D3 cells, respectively) were used. Cells were grown to confluence in α-MEM culture medium containing 10% FBS (Atlas Biologicals, Fort Collins, CO), 0.05% penicillin/streptomycin, and 400 µg/mL G418. Membranes were prepared according to the procedures described for D1R-expressing cells using D2R/D3R binding buffer (50 mM Tris containing 120 mM NaCl, 5 mM KCl, 1.5 mM $CaCl_2$, 4 mM $MgCl_2$, 1 mM EDTA, pH 7.4). One confluent 150 mm plate of D2R-expressing cells, resuspended in 10 mL of binding buffer, yielded enough membranes for 96 wells with ~10-15 µg protein/well; a single plate of D3R-expressing cells, resuspended in 15 mL, yielded sufficient membranes for 144 wells with ~7-10 µg protein/well. Cell homogenate (100 µL) was added to wells containing 800 µL of BrMeI or buffer. After 10 min, 100 µL of [^{3}H]YM-09151-2 radioligand (0.2-0.5 nM final concentration) was added and incubated at 25°C for 60 min. Reactions were stopped by filtration through polyethylenimine-soaked (0.05%) filters using a Tomtec 96-well harvester. Radioactivity on the filters was counted using a Perkin Elmer MicroBeta scintillation counter. Nonspecific binding was determined with 1 µM chlorpromazine.

[^{3}H]YM-09151-2 D4R binding assay. Human embryonic kidney (HEK) cells co-expressing the human D4.4 receptor and adenylate cyclase type I (HEK-D4.4-AC1) were used. Cells were grown

in DMEM supplemented with 5% FCS, 5% bovine calf serum (BCS), 0.05% penicillin/streptomycin, 2 µg/mL puromycin, and 200 µg/mL hygromycin. One confluent 150 mm plate yielded membranes sufficient for 144 wells with ~7-10 µg protein/well. Cells were scraped and centrifuged at 500 x *g* for 5 min. The pellet was overlaid with 2 mL binding buffer (50 mM Tris, 120 mM NaCl, 5 mM KCl, 1.5 mM $CaCl_2$, 4 mM $MgCl_2$, 1 mM EDTA, pH 7.4) and stored at -70°C until use. On the experimental day, the pellet was homogenized in assay buffer with a polytron. Cell homogenate (100 µL) was added to wells containing 800 µL of either BrMeI or binding buffer. After 10 min, 100 µL [^{3}H]YM-09151-2 (0.2-0.3 nM final concentration) was added. Plates were incubated at 25°C for 60 min. Reactions were terminated by filtration through polyethylenimine-soaked (0.05%) filters via a Tomtec 96 well harvester. Filter radioactivity was counted using a Perkin Elmer MicroBeta scintillation counter. Nonspecific binding was determined with 1 µM haloperidol.

DA receptor binding standards. Specificity of radioligand binding at the respective dopamine receptors was measured via non-radiolabeled standards. For D1R binding assays, inhibition of specific [^{3}H]SCH-23390 receptor binding was measured using cold SCH-23390 (100 nM, 10 µM). For D2R and D3R binding assays, inhibition of specific [^{3}H]YM-09151-2 receptor binding was measured with cold butaclamol (100 nM, 10 µM). For D4R binding assays, inhibition of specific [^{3}H]YM-09151-2 receptor binding was measured using cold haloperidol (100 nM, 10 µM). Inhibition of specific DA receptor binding by the respective standards is summarized in Supplementary Table 5.

Serotonin receptor binding assays

[^{3}H]8-OH-DPAT 5-HT$_{1A}$ receptor binding assay. HEK cells expressing the human 5-HT$_{1A}$ receptor (HEK-h5HT1a) were used. Cells were grown to confluence on 150 mm plates in DMEM containing 10% FCS (HyClone), 0.05% penicillin/streptomycin, and 300 µg/mL G418. Cells were collected via scraping into phosphate-buffered saline (PBS) and centrifuged at 270 x *g* for 10 min.

The cell pellet was subsequently homogenized in 50 mM Tris-HCl (pH 7.7) with a polytron, and centrifuged at 27000 × *g*. The homogenization and centrifugation were repeated to wash any remaining serotonin (5-HT) from the growth media. The final pellet was resuspended at 0.5 mg protein/mL in assay buffer (25 mM TrisHCl, 100 µM ascorbic acid, 10 µM pargyline, pH 7.4). The assay was performed in triplicate in a 96-well plate. The reaction mixture contained BrMeI, 100 µL of cell homogenate (0.05 mg protein/well) and 100 µL of [^{3}H]8-OH-DPAT (0.5 nM final concentration, 170 Ci/mmol, Perkin Elmer) in a final volume of 1 mL. Plates were incubated at room temperature for 60 min and then filtered through polyethylenimine-soaked (0.05%) filters on a Tomtec cell harvester. Filters were then washed with cold 50 mM Tris buffer (pH 7.7) for 6 sec, dried, spotted with scintillation cocktail, and counted for 2 min after a 4 hr delay on a Perkin Elmer Betaplate 1205 liquid scintillation counter (Perkin Elmer). Nonspecific binding was determined with 1.0 µM dihydroergotamine.

[^{125}I]DOI 5-HT$_{2A}$ and 5-HT$_{2C}$ receptor binding assays. This assay was adapted from previously described studies[58]. Briefly, HEK cells expressing the human 5-HT$_{2A}$ receptor (HEK-h5HT2A) or human 5-HT$_{2C}$ receptor (HEK-h5HT2C) were used. The cells were grown until confluency on 150 mm plates. Cells were washed with PBS, scraped into 2 mL PBS, and stored at -20°C until use. On the experimental day, the cell suspension was thawed and 10 mL assay buffer (50 mM Tris, pH 7.4 at 37°C, with 0.1% ascorbic acid and 5 mM $CaCl_2$) was added. This was followed by homogenization via polytron for 5 sec. The homogenate was centrifuged at 15500 rpm for 20 min. To minimize the residual 5-HT concentration, the pellet was resuspended in buffer, homogenized by polytron, and centrifuged as above. The final pellet was resuspended in 10 mL buffer/plate. For the radioligand binding studies, the binding assay included 50 µL BrMeI, 5-HT or buffer, 50 µL cell homogenate, 25 µL [^{125}I]DOI (~0.05 nM) and buffer (final volume = 250 µL). Specific binding was defined as the difference between total binding and binding in the presence of 10 µM 5-HT. The reaction was incubated for 1 hr at 37°C and terminated by filtration thru Perkin Elmer

A filtermats presoaked in 0.05% polyethylenimine using a Tomtec 96-well harvester. Remaining filter radioactivity was counted via a Perkin Elmer Betaplate 1205 liquid scintillation counter.

5-HT receptor binding standards. Specificity of radioligand binding at the respective 5-HT receptors was measured via non-radiolabeled standards. For 5-HT_{1A} receptor binding assays, inhibition of specific receptor binding was measured using cold WAY 100,635 (100 nM, 10 µM). For 5-HT_{2A} receptor binding assays, inhibition of specific receptor binding was measured with cold ketanserin (100 nM, 10 µM). For 5-HT_{2C} receptor binding assays, inhibition of specific receptor binding was measured using cold SB 242,084 (100 nM, 10 µM). Inhibition of specific 5-HT receptor binding by the respective standards is summarized in Supplementary Table 6.

Opioid receptor binding assays

Sample preparation. Receptor binding studies were conducted on CHO cells expressing µ-, κ-, or δ-opioid receptors. Rat µ-opioid receptor-expressing cells were provided by Dr. Thomas Murray (CHO-MOR) and human κ-, and δ-opioid receptor-expressing cells were provided by SRI International (CHO-KOR and CHO-DOR). CHO-MOR and CHO-KOR cell lines were maintained in DMEM supplemented with 10% FBS (Atlas Biologicals) and either 400 µg/ml or 200 µg/ml G418, respectively. CHO-DOR cells were maintained in DMEM supplemented with 10% FCS and 200 µg/mL G418. Upon reaching confluence, cells were harvested for membrane preparation. Cell membranes were prepared in 50 mM Tris buffer (pH 7.5 at 4°C). Cells were collected via scraping and centrifuged at 500 x *g* for 15 min. The cell pellet was homogenized in 2 mL buffer via polytron, diluted with 11 mL buffer, and centrifuged at 40000 x *g* for 15 min. The homogenized pellet was washed and recentrifuged, and finally resuspended at 3 mg protein/mL in buffer to determine protein content. Homogenates were stored at -70°C until use.

Binding assays. Binding assays were conducted using [^{3}H]DAMGO (0.6 nM), [^{3}H]U69,593 (0.8 nM), or [^{3}H]DPDPE (0.5 nM)**,** at the µ-, κ-, and δ-opioid receptors, respectively. The assay was

performed in triplicate in a 96-well plate using 50 mM Tris buffer (pH 7.7, room temperature). Nonspecific binding was determined with 1 μM of unlabeled radioligand. Cell membranes were incubated with the appropriate radioligand and test compound at 25°C for 60 min. Incubation was terminated by rapid filtration through glass fiber filter paper presoaked in 0.1% polyethylenimine on a Tomtec cell harvester. Filters were dried and spotted with scintillation cocktail before counting for 2 min on a Perkin Elmer microBetaplate 1450 liquid scintillation counter. Nonspecific binding was determined with 1 μM of the unlabeled form of each radioligand.

Opioid receptor binding standards. Specificity of radioligand binding at the respective opioid receptors was measured via non-radiolabeled standards. For δ- and μ-opioid receptor binding assays, inhibition of specific receptor binding was measured using naltrexone (100 nM, 10 μM). For κ-opioid receptor binding assays, inhibition of specific receptor binding was measured with nor-BNI (100 nM, 10 μM). Inhibition of specific opioid receptor binding by the respective standards is summarized in Supplementary Table 7.

Biogenic amine transporter binding assays

Sample preparation. Assay methods were adapted from previously described studies[59]. Briefly, HEK293 cells expressing either human dopamine transporter (HEK-hDAT) or human serotonin transporter (HEK-hSERT) were cultured in DMEM supplemented with 5% FBS, 5% BCS, 0.05 U penicillin/streptomycin, and 2 μg/mL puromycin. HEK293 cells expressing human norepinephrine transporter (HEK-hNET) were cultured in DMEM supplemented with 10% FBS, 0.05 U penicillin/streptomycin, and 300 μg/ml G418. Cells were grown to 80% confluence on 150 mm dishes. To prepare cell membranes, adherent cells were washed with Ca^{2+}/Mg^{2+}-free PBS, followed by addition of lysis buffer (10 mL; 2 mM HEPES with 1 mM EDTA). After 10 min, cells were scraped from plates and centrifuged at 30000 x *g* for 20 min. The pellet was resuspended in 0.32 M sucrose using a polytron homogenizer for 10 sec. The resuspension volume was

dependent on the density of binding sites and was chosen to reflect binding of 10% or less of the total radioactivity.

Binding assays. Each assay tube contained 50 µL of membrane preparation (~10-15 µg of protein), 50 µL of compound used to define non-specific binding, or buffer (Krebs-HEPES, pH 7.4; 122 mM NaCl, 2.5 mM $CaCl_2$, 1.2 mM $MgSO_4$, 10 µM pargyline, 100 µM tropolone, 0.2% glucose and 0.02% ascorbic acid, buffered with 25 mM HEPES), 25 µL of [^{125}I]RTI-55 (40-80 pM final concentration) and additional buffer sufficient to bring the final volume to 250 µL. Membranes were preincubated with drug for 10 min prior to the addition of the [^{125}I]RTI-55. Assay tubes were incubated at 25°C for 90 min. Binding was terminated by filtration over GF/C filters using a Tomtec 96-well cell harvester. Filters were washed for 6 sec with ice-cold saline. Scintillation fluid was added to each square and remaining filter radioactivity was determined using a Perkin Elmer µ- or beta-plate reader. Specific binding was defined as the difference in binding observed in the presence and absence of 5 µM mazindol (HEK-hDAT, HEK-hNET) or 5 µM imipramine (HEK-hSERT). Two independent competition experiments were conducted with triplicate determinations.

Biogenic amine transporter binding standard. Specificity of radioligand binding at the respective opioid receptors was measured via non-radiolabeled cocaine (100 nM, 10 µM). Inhibition of specific transporter binding is summarized in Supplementary Table 8.

Off-target *in vitro* binding screen

A broad receptor and enzyme target binding screen to identify potential off-target BrMeI binding was performed commercially (Eurofins Cerep Panlabs, France) as described previously[60]. BrMeI was screened at 100 nM and 10 µM concentrations with each experiment conducted in duplicate. Membrane homogenates from stable cell lines expressing each receptor or enzyme (primarily human) were incubated with the respective radioligand in the presence of either BrMeI or

reference control compounds. Respective reference compounds were tested concurrently with the test compound to assess assay reliability. Nonspecific binding for each target was ascertained in the presence of the specific agonist or antagonist. Following incubation, samples were vacuum-filtered through glass fiber filters, rinsed with ice-cold buffer using a 48-sample or 96-sample cell harvester, and filter radioactivity was measured via scintillation counter. Binding was calculated as % specific binding inhibition for each target.

hERG channel activity assay

BrMeI was commercially evaluated for activity at the hERG (encoded by the human ether-a-go-go gene) K^+ channel for potential cardiac toxicity (Eurofins Panlabs, Redmond, WA) similar to previous studies[61]. hERG K^+ channel tail current was measured by the automated patch clamp (Qpatch 16) approach[62]. CHO-KI cells stably transfected with human hERG cDNA were used for the assay. Cells were harvested via trypsinization and maintained in serum-free medium at room temperature prior to recording. Cells were washed and resuspended into extracellular solution (137 mM NaCl, 4 mM KCl, 1.8 mM $CaCl_2$, 1 mM $MgCl_2$, 10 mM D(+)-glucose, 10 mM HEPES, pH 7.4). For recordings, the intracellular pipette solution consisted of 130 mM KCl, 10 mM NaCl, 1 mM $MgCl_2$, 10 mM EGTA, 5 mM MgATP, 10 mM HEPES (pH 7.2). Upon achieving a whole cell configuration, cells were held at -80 mV. A 50 ms pulse to -40 mV was delivered to measure the leaking current which was subtracted from the tail current. Cells were subsequently depolarized to +20 mV for 2 sec, followed by a 1 sec pulse to -40 mV to induce tail currents. This recording procedure was repeated every 5 sec to monitor current amplitude. Tail current amplitudes were measured in response to different BrMeI concentrations (0.01-100 μM, in DMSO) applied sequentially. All experiments were performed at room temperature in duplicate. The reference compound control E-4031 was tested in parallel at multiple concentrations to obtain an IC_{50} curve. Data were analyzed to yield the % hERG channel inhibition by comparing tail current amplitude prior to and following BrMeI application; the current difference was normalized to control. Dose-

response curves were fit via 3-parameter logistic regression of Log[drug] concentration to generate IC_{50} values for BrMeI-induced hERG channel inhibition.

Mouse microsomal stability assay

Phase I metabolic stability assays were carried out in mouse liver microsomes as previously described[63]. Reactions were carried out with 100 mM potassium phosphate buffer, pH 7.4, in the presence of the NADPH regenerating system (1.3 mM NADPH, 3.3 mM glucose 6-phosphate, 3.3 mM $MgCl_2$, 0.4 U/mL glucose-6-phosphate dehydrogenase, 50 µM sodium citrate). Reactions, conducted in triplicate, were initiated via addition of liver microsomes to the incubation mixture (1 µM compound final concentration; 0.2 mg/mL microsomes). Negative controls in the absence of NADPH system determined specific cofactor-free degradation. Compound disappearance was monitored via LC/MS/MS. Briefly, chromatographic analysis was performed using an Accela ultra high-performance system consisting of an analytical pump, and an autosampler coupled with a TSQ Vantage mass spectrometer (Thermo Fisher Scientific). Separation of the analyte from potentially interfering material was achieved at ambient temperature using an Agilent Eclipse Plus column (Agilent, Santa Clara, CA; 100 x 2.1mm i.d.) packed with a 1.8 µm C18 stationary phase. Mobile phase was composed of 0.1% formic acid in acetonitrile and 0.1% formic acid in water with gradient elution, starting with 10% (organic) linearly increasing to 99% up to 2.5 min, maintaining at 99% (2.5-3.5 min) and re-equilibrating to 10% by 4.5 min. The total run time for each analyte was 5.0 min.

***In vivo* rodent studies**

Animal husbandry. Animals were housed in accordance with NIH guidelines along with ARRIVE guidelines for reporting animal research[64, 65]. Mice and rats were housed in cages with a 12:12 light:dark cycle and had access to food and water *ad lib* at all times unless indicated otherwise. All efforts were made to ameliorate animal suffering.

Institutional approvals. All animal work was approved through the Institutional Animal Care and Use Committees at the University of Pittsburgh, Albert Einstein College of Medicine, Johns Hopkins University, and the University of Toronto.

Sex as a biological variable. Only male rodents were used to avoid the impact of estrus on hormone secretion and islet physiology. Additionally, our choice was based on recent work showing that male rodent β-cells possess transcriptomic signatures more similar to T2D compared to females[66, 67].

***In vivo* pharmacokinetics.** All pharmacokinetics assays were conducted in 6-8-week-old male CD1 mice (Harlan, Indianapolis, IN) weighing 20-25 g using similar methods to those described earlier[68-70]. BrMeI and unmodified bromocriptine were dosed at 10 mg/kg intravenously (i.v.) with dosing based on earlier metabolic studies in rodents[5, 71, 72]. Following administration, blood was collected via cardiac puncture at 15 min and 1 h post-dose (n=3 mice/time point). Plasma was harvested from blood by centrifugation at 3000 x *g*. Whole brains were collected, and all samples were stored at -80°C until analysis. Samples were extracted from the plasma using a one-step protein precipitation method with acetonitrile containing losartan (500 nM) as an internal standard. Extracts were vortexed and then centrifuged at 10000 x *g* (10 min, 4°C). For analysis of analytes in brain, whole brains were weighed and homogenized in 4 times the volume of acetonitrile (also containing internal standard losartan), followed by vortexing and centrifugation for sample extraction Once extracted, aliquots of the plasma and brain samples were diluted with water, transferred to a 250 µL polypropylene vial sealed with a Teflon cap, and analyzed via LC/MS/MS. Chromatographic analysis was performed on an Accela ultra high-performance system consisting of an analytical pump, and an autosampler coupled with TSQ Vantage mass spectrometer (see Supplementary Figure S5). Calibration standards were prepared from naïve mouse plasma or brain samples spiked with known concentrations of BrMeI and unmodified bromocriptine. Plasma concentrations (nmol/mL) and brain tissue concentrations (pmol/g) of the respective drugs were ascertained and plotted at the respective time points.

Diet. 3-4-month-old wild-type C57BL/6J mice used in the glucose and insulin tolerance tests were fed a Western diet (5TJN: 40% fat, 44% carbohydrate, 16% protein; TestDiet) whose composition is analogous to previously described formulations[73, 74]. Animals were fed this Western diet for 12 weeks alongside drug administration.

Drug administration. Bromocriptine and BrMeI were dissolved in a solution of 50% DMSO in water (50% DMSO/50% dH_2O) to a final concentration of 2 mg/mL and administered to mice i.p. Vehicle was defined as 50% DMSO/50% dH_2O only. For glucose and insulin tolerance testing in mice, animals were administered the respective drugs or vehicle for 12 weeks via daily intraperitoneal (i.p.) administration. In a subset of glucose tolerance testing (GTT) studies, mice were administered either bromocriptine or vehicle daily via an intracerebroventricular (i.c.v.) route for 8 weeks prior to testing. At the 8-week time point, bromocriptine GTT data was compared between i.c.v. versus systemic bromocriptine administration. As a control, 8 weeks of systemic bromocriptine was sufficient to improve glucose tolerance in dysglycemic Western diet-fed mice (data not shown). All i.p. and i.c.v. treatments were conducted at the same time of day to control for potential circadian effects.

Intracerebral ventricular drug administration in mice. I.c.v. drug administration in adult mice was conducted as described earlier[75]. Mice were anesthetized with ketamine/xylazine for implantation of custom indwelling 3.5 mm guide cannulas (Plastics One Inc., Roanoke, VA) into the third cerebral ventricle using a stereotaxic apparatus (coordinates from bregma: anteroposterior, -0.3 mm; dorsoventral, -3 mm). Mice were allowed to recover for at least a week prior to i.c.v. drug administration.

Glucose tolerance testing. Oral glucose tolerance testing (OGTT) was conducted as previously described[75]. Briefly, Western diet-fed wild-type C57BL/6J on Western diet underwent a 6-h daytime fast (food away at 8AM, OGTT at 2PM) followed by a glucose challenge with a glucose load of 2 mg/kg (10% glucose stock). Glucose measurements were made from tail vein blood samples drawn at 0, 15-, 30-, 60- and 120-min following glucose challenge. Samples were

measured immediately in duplicate using Contour glucometer sticks (Bayer Corp., Whippany, NJ).

Insulin tolerance testing. Western diet-fed wild-type C57BL/6J mice underwent a 6-h daytime fast, which was followed by intraperitoneal administration of 1.5 U/kg human insulin. Glucose values were determined from blood collected at 0, 15-, 30-, 60- and 120-min following insulin administration via tail bleed. Blood glucose samples were measured immediately in duplicate using Contour glucometer sticks. Insulin was measured in parallel via a quantitative ELISA kit (Linco Research Inc., St. Charles, MO).

Intracerebroventricular L-DOPA studies in rats. Male Sprague-Dawley rats underwent intracerebroventricular (i.c.v.; 3rd ventricle) surgeries as described previously[20, 76]. A cannula was stereotaxically placed into the third cerebral ventricle under isoflurane anesthesia (coordinates from bregma: anteroposterior, -2.5 mm; mediolateral, 0.0 mm; dorsoventral, -8.0 mm). The cannula was secured in place with stainless steel screws (McCray Optical Supply Inc., Scarborough, ON, Canada) and dental cement, and kept patent with a steel stylet. Following approximately 1 week of recovery, rats underwent blood vessel cannulation for future blood sampling as earlier[20]. Rats were monitored closely after surgeries with behavior and body weight recorded daily to ensure successful recovery. Following ~4 days of recovery from the last surgery, rats were food-restricted overnight and then infused (5 µL/h) i.c.v. with 10 mM L-DOPA or vehicle (saline) for 3.5 h. Acute potential changes in glycemic control were determined via periodic measurement of plasma glucose 0, 60-, 90-, 190-, 200-, and 210-min with a glucose analyzer (Analox Instruments, Stourbridge, UK). Plasma insulin was measured via ELISA (Mercodia, Winston Salem, NC).

Statistics

Data are represented as means ± SEM for all experimental replicates. We used multi-factor analyses of variance (ANOVA; α = 0.05) to compare between-group differences. This included

repeated measures two-way ANOVAs to compare between-group differences in glucose and insulin tolerance tests; Tukey's multiple comparison tests were conducted for multiple post hoc comparisons. Statistical analyses were performed with GraphPad Prism. Significance was accepted at $p < 0.05$.

Results

Design and synthesis of quaternary MeI analogues of DA D_2-like receptor-targeted drugs

We aimed to establish a family of pharmacological tools to selectively manipulate DA D_2-like receptor signaling in the periphery while limiting their actions in the CNS. Based on earlier approaches employing MeI quaternization to produce peripherally-limited drugs[77-80], we hypothesized that addition of a quaternary MeI group would similarly render D_2-like receptor agonists less BBB-permeable. We first synthesized quaternary MeI salts of full D_2-like receptor agonists that broadly target both D2R and D3R including (-)-quinpirole (**Figure 1A**) and bromocriptine (**Figure 1B**), producing MeI analogues AB01-59 and AB01-60, respectively. To focus more specifically on D2R, we quaternized sumanirole, a D2R-selective agonist, to generate MPE01-05 (**Figure 1C**). We also synthesized MeI analogues of D3R-preferential agonists (±)-7-OH-DPAT (AB01-62, **Figure 1D**) and (+)-PD128,907 (AB01-117, **Figure 1E**). To target peripheral D4R, we generated a quaternary MeI analogue of CAB03-015, a D4R-selective agonist[51] (AB01-102, **Figure 1F**). Additionally, we synthesized an MeI analogue of aripiprazole which is a D_2-like receptor partial agonist and is in clinical use as an APD[81, 82] (AB01-61, **Figure 1G**). Finally, we generated an MeI analogue of a D_2-like receptor antagonist by quaternizing L741,226 (MPE01-06, **Figure 1H**). Following synthesis, the respective MeI-modified compounds were evaluated to be >95% pure based on NMR, elemental analysis, HRMS (high resolution mass spectroscopy which agrees within ± 5 ppm) and MS/MS (ESI in positive mode) (**Supplementary Table 1**).

Characterization of D_2-like receptor binding properties of MeI analogues

We ascertained whether MeI quaternization altered the D_2-like receptor binding affinities of the MeI analogues by measuring dissociation constant (K_i) values. Overall, the absolute K_i values were higher for all MeI analogues at human D2R and D3R compared to their respective parent compounds when in competition with agonist radioligand [^{3}H]-(R)-(+)-7-OH-DPAT (**Table 1**). Nevertheless, some MeI analogues exhibited greater alterations in D2R and D3R binding affinities compared to others. For example, the MeI analogue of bromocriptine, AB01-60, continued to bind to D2R and D3R with relatively high affinity, demonstrating only 5.3-fold and 8.5-fold diminished affinities at D2R and D3R, respectively, compared to its unmodified parent compound. In contrast, the MeI analogue of (±)-7-OH-DPAT, AB01-62, showed 179-fold and 365-fold decreased binding affinity at D2R and D3R versus unmodified (±)-7-OH-DPAT. Just as importantly, MeI modification altered the relative balance of D2R versus D3R binding affinities for some of the analogues, while leaving others unchanged. AB01-59 showed preferential binding to D2R over D3R compared to unmodified (-)-quinpirole as indicated by a 6.3-fold-increase in the D3R/D2R ratio. In contrast, AB01-102, AB01-61, and MPE01-06 showed increased D3R affinity versus D2R (**Table 1**), suggesting that local changes in polarity following MeI addition may play a key role in determining D2R/D3R receptor binding properties. Finally, we measured the binding affinities of D4R-selective agonist CAB03-015 and its MeI analogue AB01-102 at human D4R, finding a 61.7-fold loss of binding affinity for AB01-102 compared to its unmodified parent (**Supplementary Table 2**).

Functional characterization of MeI analogues

We evaluated the activity of our MeI analogues via the mitogenesis functional assay, where we measured D_2-like receptor-mediated increases in the incorporation of [^{3}H]thymidine in CHO cells expressing either human D2R or D3R[53] (**Figure 2**). The canonical D2R/D3R agonists (-)-quinpirole and bromocriptine and their respective MeI analogues produced robust concentration-

dependent D2R- and D3R-mediated increases in [^{3}H]thymidine incorporation (**Figures 2A-2D**). However, while the efficacies of both AB01-59 and AB01-60 were largely unchanged compared to their respective unmodified parents, AB01-59 displayed diminished potency in inducing D2R- and D3R-mediated mitogenesis (24.9-fold, D2R; 14.4-fold, D3R) compared to AB01-60 (15.6-fold, D2R; 11.2-fold, D3R) (**Table 2**). Notably, MPE01-05, the MeI analogue of sumanirole, did not drive significant changes in either efficacy or potency in D2R- and D3R-mediated mitogenesis (**Figures 2E, 2F**). In contrast, AB01-62 and AB01-117, MeI analogues of preferential D3R agonists, demonstrated substantial loss of potency in D3R-mediated mitogenesis (AB01-62: 1107.4-fold decrease; AB01-117: 60.3-fold decrease) despite retaining their efficacies (**Figures 2G, 2H, Table 2**). Consistent with aripiprazole's partial agonism of D2R and D3R, MeI analogue AB01-61 also displayed partial agonist properties in D2R- and D3R-mediated mitogenesis with near-identical efficacies. However, AB01-61 showed markedly reduced potencies compared to aripiprazole (D2R, 1605.3-fold decrease; D3R, 90.7-fold decrease), suggesting that this analogue has little functional activity at either D2R or D3R (**Figures 2I, 2J, Table 2**). As expected, MPE01-06, the MeI analogue of D2R/D3R antagonist L741,626, had no significant functional effects on mitogenesis in our assay (<1% of the maximum (-)-quinpirole response; **Figures 2K, 2L, Table 2**). Lastly, since CAB03-015 is a D4R-selective agonist, we tested the activity of the drug and its MeI analogue AB01-102 in a D4R-mediated adenylate cyclase activity/cyclic AMP (cAMP) formation assay. Both drugs behaved as partial agonists, exhibiting similar efficacies in eliciting D4R-driven decreases in forskolin-stimulated adenylate activity and the resulting cAMP formation. However, AB01-102 showed strongly diminished potency (731.9-fold decrease) compared to unmodified CAB-03-015 (**Supplementary Table 3**).

MeI analogues modify glucose-stimulated insulin secretion

We and our colleagues previously showed that human and rodent insulin-secreting pancreatic β-cells expressed D_2-like receptors including D2R and D3R, and that agonist stimulation of these receptors by (-)-quinpirole and bromocriptine decreased glucose-stimulated insulin secretion (GSIS)[9, 12, 13, 27-29, 57, 83, 84]. Therefore, we further functionally tested the ability of several of the MeI analogues to directly signal through β-cell D_2-like receptors by examining their impact on GSIS in INS-1E cells, an insulin-secreting rat pancreatic β-cell line[55]. As expected, unmodified (-)-quinpirole and bromocriptine dose-dependently reduced GSIS [(-)-quinpirole IC_{50} = 1.18 μM; bromocriptine IC_{50} = 0.18 μM] (**Figures 3A, 3B, Table 3**). AB01-59, the MeI analogue of (-)-quinpirole, similarly decreased GSIS, but with reduced efficacy (48.4% decrease) and potency (IC_{50} = 6.94 μM, 5.9-fold decrease) versus unmodified (-)-quinpirole (**Figure 3A, Table 3**). By comparison, bromocriptine MeI analogue AB01-60 functioned as a full agonist, completely retaining its efficacy, albeit with decreased potency (IC_{50} = 10.17 μM, 57.7-fold decrease) compared to unmodified bromocriptine (**Figure 3B, Table 3**). Interestingly, the D2R-preferential agonist sumanirole[85] or D3R-preferential PD128,907[86] and their respective MeI analogs exhibited markedly less efficacy and potency in GSIS inhibition than non-selective D2R/D3R agonists (-)-quinpirole or bromocriptine (**Figures 3C, 3D, Table 3**). This is consistent with our recent findings that both D2R and D3R must work in combination to effectively modulate GSIS[11]. Together, given AB01-60's preservation of D2R/D3R binding affinity and efficacy in both GSIS and mitogenesis assays (**Tables 2, 3**), we chose this compound (henceforth termed bromocriptine MeI or BrMeI) as our lead compound.

BrMeI preferentially recruits β-arrestin2 to D2R

We next characterized BrMeI-stimulated signaling through D2R. We focused on BrMeI's ability to initiate D2R-mediated recruitment of intracellular effectors such as G protein $G\alpha_{i1}$ and β-arrestin2, given their important metabolic roles in the regulation of hormone secretion[13, 32, 87-89]. We

employed highly sensitive nanoBRET technology to determine if BrMeI-stimulated recruitment of $G\alpha_{i1}$ and β-arrestin2 to D2R differed from that of either unmodified bromocriptine or endogenous ligand DA. In our assay, D2R was HaloTag-labeled with a bright fluorescent dye and either $G\alpha_{i1}$ or β-arrestin2 was tagged with nanoluciferase (NanoLuc). In response to receptor recruitment, the resulting proximity of the receptor-effector pair enables luminescence from the NanoLuc-tagged effector to excite the receptor-bound dye, generating quantifiable fluorescence[90]. D2R stimulation by DA caused dose-dependent recruitment of $G\alpha_{i1}$ (EC_{50} = 288.67 nM). Bromocriptine was much more potent than DA at eliciting $G\alpha_{i1}$ recruitment to D2R (EC_{50} = 15.07 nM), albeit with 47% less efficacy. This suggested that bromocriptine functioned as a partial agonist in eliciting $G\alpha_{i1}$ recruitment to D2R. BrMeI's efficacy resembled unmodified bromocriptine, though with less potency (EC_{50} = 1514.71 nM) (**Figure 4A, Supplementary Table 4**). Importantly, we discovered that BrMeI more potently elicited β-arrestin2 recruitment to D2R (EC_{50} = 8.37 nM) compared to bromocriptine (EC_{50} = 20.13 nM) and DA (EC_{50} = 27.63 μM), while still retaining bromocriptine's reduced efficacy (**Figure 4B, Supplementary Table 4**). These data suggest that BrMeI is an agonist of D2R that preferentially recruits β-arrestin2 over G proteins to D2R.

In vitro target binding profile of BrMeI

We further characterized BrMeI's binding specificity in a series of *in vitro* radioligand binding competition assays via an initial screen for binding to several families of G protein-coupled receptors (*e.g.*, DA, serotonin, opioid receptors) and biogenic amine transporters. Radioligand binding was successfully validated using established standards (**Supplementary Tables 5-8**). At submicromolar concentration (100 nM), BrMeI did not exhibit significant screen hits (**Supplementary Figure 1**). However, at a higher concentration (10 μM), BrMeI demonstrated strong D2R and D3R binding (92.2% and 99.0% inhibition of specific radioligand binding, respectively), consistent with its potencies in the GSIS and mitogenesis assays. In contrast, BrMeI

did not significantly bind to D1R or D4R (**Supplementary Figure 1**). We additionally observed significant BrMeI binding to serotonin 5-HT_{1A}, 5-HT_{2A}, and 5-HT_{2C} receptors as well as to δ-, κ-, and μ-opioid receptors at the 10 μM concentration, which is in line with bromocriptine's ability to similarly bind other receptors[41]. We found no biogenic amine transporter binding at either tested BrMeI concentrations (**Supplementary Figure 1**).

We next conducted a larger screen to detect potential off-target binding by BrMeI across a broad range of human receptors, channels, and enzymes. As above, we found no significant hits at the lower submicromolar 100 nM BrMeI concentration (**Supplementary Figure 2, Supplementary Figure 3**). At the higher 10 μM concentration, we identified BrMeI binding to α_2 adrenergic receptors, consistent with work showing bromocriptine's ability to signal via both D_2-like and α_2 adrenergic receptors[12, 91, 92]. At 10 μM BrMeI, we also found positive hits at A_{2A}, α_1, α_2, $D_{4.4}R$, κ-opioid, μ-opioid, M, M_2, NK_1, and NK_2 receptors, L-type Ca^{2+} (diltiazem) and Na^{+} (site 2) channels as well as acetylcholinesterase (**Supplementary Figure 2, Supplementary Figure 3**). Finally, we tested BrMeI for hERG channel activity, finding concentration-dependent hERG tail current inhibition (IC_{50} = 8.65 μM) (**Supplementary Figure 4**), consistent with similar hERG activity by unmodified bromocriptine[93].

BrMeI undergoes Phase I metabolism in mouse microsomes identically to bromocriptine

We tested BrMeI for Phase I metabolic stability using mouse liver microsomes fortified with NADPH, comparing its stability to unmodified bromocriptine; fractions of drug remaining over time were measured via LC/MS/MS[70]. Incubation of BrMeI and bromocriptine in the presence of NADPH led to the complete disappearance of bromocriptine within 30 min (**Figure 5A**). Similarly, we found almost complete BrMeI loss within 30 min and total loss by 60 min (**Figure 5B**). These

results indicate that BrMeI undergoes significant hepatic metabolism in a manner identical to unmodified bromocriptine.

Pharmacokinetic evaluation of BrMeI *in vivo*

We evaluated the pharmacokinetics of BrMeI versus unmodified bromocriptine *in vivo* in wild-type CD1 mice. Mice were administered 10 mg/kg BrMeI or bromocriptine via an intravenous (i.v.) route followed by LC/MS/MS measurements of plasma and brain drug levels 15- and 60-min post-administration (**Figure 5C-E, Supplementary Figure 5, Table 4**). At 15 min, the brain/plasma ratio for BrMeI was 2.5-fold lower compared to bromocriptine, suggesting that, acutely, BrMeI had lower brain penetrance and was preferentially localized to the periphery (**Figures 5C, 5D**). However, by 60 min, the brain/plasma ratios of BrMeI and bromocriptine were similar (bromocriptine, 0.45; BrMeI, 0.51), suggesting that BrMeI was not completely restricted from the CNS (**Figure 5E**). Rather, quaternary MeI modification significantly slowed BBB penetration of the drug. Importantly, by 60 min post-administration, most unmodified bromocriptine was cleared from both brain (92.9% decrease) and plasma (88.2% decrease) *in vivo* (**Table 4**). In contrast, significantly higher plasma and brain levels of BrMeI still remained at this later timepoint (**Figure 5**). Indeed, plasma BrMeI levels were ~8-fold greater compared to bromocriptine at 60 min, suggesting that BrMeI possessed an *in vivo* pharmacokinetic profile distinct from unmodified bromocriptine which enabled increased duration of action.

Actions at both CNS and peripheral targets are required to effectively treat dysglycemia *in vivo*

Finally, we examined the metabolic impacts of BrMeI versus bromocriptine on systemic glucose homeostasis *in vivo* in a diet-induced obesity (DIO) model of T2D where wild-type C57BL/6J mice were chronically maintained on a Western diet to induce dysglycemia and obesity. As expected,

vehicle-treated control mice exhibited fasting hyperglycemia and impaired glucose tolerance during oral glucose tolerance testing (OGTT). We discovered that systemic administration of bromocriptine produced significant improvements in glucose tolerance as indicated by a significant effect of drug [$F(2, 29) = 13.10$, $p < 0.0001$] as well as an interaction of drug $\times$ time [$F(8, 116) = 4.178$, $p = 0.0002$]. In contrast, systemic administration of BrMeI did not significantly modify glucose tolerance compared to vehicle ($p > 0.05$) (**Figure 6A**). Systemic drug treatment also lowered fasting blood glucose [$F(2, 29) = 6.994$, $p = 0.0033$]. While bromocriptine-treated mice exhibited significantly lower fasting glucose, BrMeI treatment had no significant effect ($p > 0.05$) (**Figure 6B**). Insulin tolerance testing (ITT) similarly revealed a significant effect of drug treatment on blood glucose [$F(2, 21) = 6.761$, $p = 0.0054$] driven by bromocriptine-induced improvements in insulin sensitivity (**Figure 6C**). Notably, systemic BrMeI's effects on blood glucose during the ITT were intermediate to those of bromocriptine and vehicle. BrMeI significantly reduced blood glucose versus vehicle at the 60 min time point ($p = 0.022$, **Figure 6C**), suggesting that the drug may have partial efficacy on improving insulin sensitivity *in vivo*. We also measured the impact of systemic bromocriptine and BrMeI treatment on blood insulin during the initial 15 min of the ITT time course. There was a significant drug $\times$ time interaction [$F(4, 42) = 10.57$, $p < 0.0001$] on blood insulin driven by bromocriptine's ability to significantly enhance the levels of circulating plasma insulin within 5 min of insulin administration versus vehicle ($p = 0.0002$) or BrMeI ($p = 0.0003$); BrMeI treatment did not significantly alter plasma insulin ($p > 0.05$) (**Figure 6D**). Together, these results were consistent with bromocriptine's established role as a treatment for dysglycemia in T2D[42, 94, 95]. Interestingly, neither systemic bromocriptine nor BrMeI treatments had significant effects on weight at 12 weeks ($p > 0.05$) (**Figure 6E**), suggesting that drug-induced effects on dysglycemia could be dissociated from effects on weight gain.

Our *in vivo* metabolic results also raise the important question of whether the mechanisms responsible for systemic bromocriptine's improvements in dysglycemia are through its actions on targets in the CNS versus those in the periphery or via its concurrent actions at both sites. To test whether bromocriptine's effects are primarily due to CNS actions, we limited its actions to the brain via intracerebroventricular administration (i.c.v.) of the drug in Western-diet fed wild-type C57BL/6J mice. In contrast to systemic administration, i.c.v. bromocriptine had no significant effect on glucose tolerance ($p > 0.05$, **Figure 6F**). We validated these results by directly infusing DA precursor L-DOPA into the brain via i.c.v. administration in Sprague-Dawley rats for an extended 3.5-h period to permit adequate time for conversion into DA. Similar to our i.c.v. bromocriptine data, L-DOPA infusion did not significantly impact plasma glucose or insulin levels ($p > 0.05$; **Supplementary Figure 6**). Overall, these data suggest that both actions on targets in the CNS and periphery are required to effectively modify glycemic control.

Discussion

Diabetes represents one of the most widespread conditions today, affecting ~10% of the adult population of the United States[96]. Dysglycemia is central to the pathology of diabetes, resulting in a significant proportion of the morbidity and mortality associated with the illness[97, 98]. Treatment with APDs, some of the most widely prescribed psychiatric medications today, is a key contributor to the development of dysglycemia and T2D[99, 100]. Notably, though most of the focus on APDs' metabolic symptoms has been on second-generation APDs like olanzapine[101, 102], even first-generation drugs (*e.g.*, chlorpromazine and haloperidol) disrupt glycemic control, providing clues concerning the biological mechanisms underlying dysglycemia[26, 103-106]. Although multiple cellular targets for APDs have been identified[26, 37, 107-109], the single unifying property of all APDs is their blockade of D2R and D3R. Conversely, bromocriptine, a D2R/D3R agonist can reduce dysglycemia and is FDA-approved to treat T2D[42, 110]. Together, this suggests an important role for DA and D2R/D3R signaling in glycemic control and treatment of dysglycemia.

DA's emerging roles in metabolic regulation have been most extensively examined in the CNS. Significantly, both D2R and D3R are expressed in the hypothalamus, a brain region heavily involved in the homeostatic regulation of appetite and metabolism[17, 111, 112]. Indeed, hypothalamic D2R/D3R signaling mediates regulation of appetite and feeding behaviors that can result in compulsive overeating[17, 18, 113, 114]. Consistent with this, D2R blockade in the lateral hypothalamus increases food intake[17, 112, 115]. Hypothalamic D2R is expressed within arcuate nucleus neurons that are sensitive to peripheral hormone modulators of appetite and feeding including leptin and ghrelin, further linking central DA signaling to metabolic regulation, food intake and body weight changes, as well as to APD-related metabolic side effects[8, 10, 17, 19, 111, 116]. Moreover, hypothalamic D2R tonically regulates the release of prolactin, a hormone strongly associated with metabolic regulation as well as dysglycemia[117, 118]. There is also growing evidence of ongoing interplay between the CNS and periphery via leptin and ghrelin and dopaminergic mesolimbic and nigrostriatal circuits to modulate feeding[119-121]. In the striatum, D2R and D3R also modulate food-related reward, motivation, and anticipatory behaviors and are implicated in binge or compulsive eating[23, 122-124]. On the other hand, some reports suggest that CNS dopaminergic signaling in relation to feeding and reward is not sufficient to fully explain the mechanisms by which DA and D_2-like receptors modulate metabolism[26, 125]. For example, changes in glucose homeostasis in response to D2R/D3R blockade by APDs occur even in the absence of increased food intake or psychiatric disease[126, 127], and as little as a single administration of the APD olanzapine is sufficient to alter glucose homeostasis in healthy human subjects[33]. Recent discoveries that the endocrine pancreas uses local DA biosynthesis and signaling to modulate hormone release raises the intriguing possibility that dopaminergic regulation of metabolism may also rely on targets in the periphery[28, 32]. However, it has been very challenging to unravel central versus peripheral contributions of D2R/D3R signaling in metabolic regulation due to the current paucity of readily accessible pharmacological tools specifically targeting these respective compartments. Therefore, our goal was to generate a peripherally-limited D2R/D3R agonist to more selectively

examine the metabolic roles of D2R/D3R signaling within the periphery. Such a drug could also serve as a comparator to the metabolic effects of D2R/D3R signaling in the CNS.

We employed a MeI quaternization strategy to render D_2-like receptor-targeted drugs less BBB permeable. Indeed, MeI modification of compounds has been successfully used in experimental models of pruritus[128], drug intoxication[77, 79], substance dependence[129] and withdrawal[78, 130]. We identified BrMeI as our lead compound based on its preserved receptor binding affinities for D2R and D3R as well as its efficacy in several *in vitro* functional assays, albeit with reduced potency. Consistent with this, higher concentrations of BrMeI shared bromocriptine's receptor binding not only for D2R and D3R, but to additional GPCRs relevant to metabolic regulation including α_{2A} adrenergic and serotonin (5-HT_{1A}, 5-HT_{2A}, 5-HT_{2C}) receptors[12, 26, 91, 92]. These receptors are well-established modulators of metabolism[32, 131-133] and we posit that such additional targets contribute to bromocriptine's therapeutic efficacy in improving dysglycemia.

Our *in vivo* metabolic data validates bromocriptine's ability to improve dysglycemia within the established DIO model of T2D. This is consistent with extensive preclinical and clinical human data demonstrating bromocriptine's efficacy in treating T2D dysglycemia[4, 134-137]. Work from our group and others points to bromocriptine's actions in the periphery as an important component of its clinical effectiveness[12, 92]. We recently demonstrated that this drug also acts directly on peripheral dopaminergic targets including α-cell and β-cell D2R and D3R to reduce glucagon and insulin secretion[12]. Indeed, bromocriptine's actions in the periphery may improve dysglycemia by: 1) diminishing hyperglucagonemia which in turn lowers hyperglycemia; and 2) decreasing chronic hyperinsulinemia. This induces a state of β-cell rest that resensitizes insulin-sensitive tissues and reduces cytotoxic β-cell stress[12, 32]. Beyond the endocrine pancreas, bromocriptine also acts on additional peripheral targets in adipose tissue including D_2-like receptors and α_{2A} adrenergic

receptors to further improve metabolism by modifying adipokine expression as well as diminishing adipogenesis and lipogenesis[138-140]. Collectively, these findings provide a strong rationale for our use of BrMeI to not only dissect central versus peripheral mechanisms of D2R/D3R-mediated glycemic control, but to potentially serve as a therapeutic tool capable of fine-tuning peripheral metabolism without potential CNS side effects.

According to our *in vivo* pharmacokinetic assay, BrMeI was preferentially distributed to the periphery shortly following systemic i.v. administration. In contrast to our original hypothesis, we discovered that BrMeI was equally distributed between the brain and periphery 1-hr post-administration. This suggests that the MeI modification did not fully block BrMeI's entrance into the CNS over time. Nevertheless, compared to bromocriptine, BrMeI was present in the periphery as well as brain at much higher concentrations long after unmodified bromocriptine was cleared. Thus, despite its lower potency, BrMeI has a longer opportunity to signal, including in the periphery. Furthermore, BrMeI's reduced efficacy in recruiting β-arrestin2 to D2R also suggests diminished D2R internalization and desensitization, enabling extended receptor signaling.

Our *in vivo* metabolic studies comparing the impacts of systemic administration of bromocriptine and BrMeI versus i.c.v. administration of bromocriptine and L-DOPA strongly suggest that stimulation of CNS dopaminergic targets by either bromocriptine or L-DOPA is insufficient to modify glycemic control. Instead, these data point to the importance of tandem targeting of both central and peripheral targets for effective glycemic control as well as for improvements in dysglycemia. Indeed, there is evidence of coordination between the hypothalamus and the autonomic nervous system (ANS) to control energy metabolism[141, 142]. Catecholamine signaling between the CNS and liver may be critical for this coordinated metabolic signaling. Bromocriptine-induced attenuation of hypothalamic noradrenergic drive, along with a reduction in the levels of circulating sympathetic mediators, diminished gluconeogenesis and lipolysis, provides an

additional mechanism for improving dysglycemia[143, 144]. Ventromedial hypothalamic catecholamine activity was also correlated with a decrease in the hepatic transcription factors that potentiate gluconeogenesis and fatty acid oxidation after treatment with bromocriptine[5]. Finally, hypothalamic-ANS coordination mediating fat browning in relation to DA receptor agonism[3, 145, 146] may explain the lack of net effects on weight or body composition with improved glucose tolerance (*i.e.*, same fat mass, albeit with a different metabolic phenotype).

Limitations of the study include the incomplete limitation of BrMeI to the periphery with BBB penetrance over time. As a result, we cannot completely rule out that the BrMeI in the brain may contribute to the metabolic effects described here following its systemic administration. While possible, this is unlikely given the absence of significant effects in our OGTT studies. Despite sharing similar efficacies with unmodified bromocriptine in our GSIS and mitogenesis assays, it is also possible that BrMeI's diminished potency may be responsible for the lack of an effective metabolic response. Evidence of a partial *in vivo* response in our ITT assay suggests that BrMeI retains some potency. Nevertheless, future work is clearly required to create the next generation of peripherally-limited D2R/D3R agonists with tighter exclusion from the brain across time. Another limitation is the lack of functional characterization of BrMeI's actions on non-dopaminergic targets including serotonergic and adrenergic receptors. Lastly, our *in vivo* metabolic assays did not examine the impact of circadian rhythms on central and peripheral glycemic control by sampling at multiple zeitgebers, despite growing evidence of a strong circadian component to both central and peripheral dopaminergic metabolic regulation[122, 147-150] – a topic for further studies.

Besides their utility in defining CNS versus peripheral contributions of the DA system to metabolic regulation, we propose that future generations of peripherally-limited D2R/D3R agonists can serve as especially effective treatments for APD-induced dysglycemia. Because APD-induced

D2R/D3R antagonism is not limited to the CNS, these medications can act on peripheral dopaminergic targets to cause and/or exacerbate dysglycemia[26, 32, 37, 151]. As a result, co-administration of a D2R/D3R agonist whose actions are limited to the periphery would outcompete peripheral APD actions. Such a strategy would offset or overcome APD-induced dysglycemia with minimal risk of CNS/psychiatric side effects and without interfering with APDs' intended therapeutic actions in the CNS.

Together, our results suggest that coordinated signaling via CNS and peripheral D_2-like receptors is required for bromocriptine's metabolic effects and underscores the importance of both peripheral and CNS dopaminergic metabolic regulation. Moreover, the design of peripherally-limited dopaminergic agonists opens the door to new classes of drugs for better, more effective treatment of dysglycemia.

Data availability

All data will be made available by the corresponding author upon request.

Author contributions

Synthesis and characterization of test chemicals were performed by AB, ME, CAB, JD, and AHN. Mitogenesis assays were performed by AJE and AJ. Insulin secretion assays were performed by ZJF. NanoBRET assays were performed by DA. Metabolic stability and pharmacokinetic studies were performed by RR and BSS. Rodent metabolic studies were performed by SP, MKH, and GJS. AB, JOMR, GJS, AHN, and ZF wrote the manuscript. Manuscript review and editing were performed by AB, ME, ZJF, DA, RR, SP, JOMR, CAB, BSS, AJE, AJ, MKH, GJS, AHN, and ZF. Project administration and supervision were provided by ZF.

Acknowledgments

We gratefully thank Drs. Jeffrey Deschamps, Caitlin Burzynski, Jonathan Javitch, Vijay Yechoor, and George Gittes for assistance and helpful discussions throughout these studies. Funding support was provided by NIH grant R01DK124219 (ZF), K08DA031241 (ZF), DP1DA058385 (CAB), Department of Defense grants PR141292 (ZF, GJS), PR210207 (ZF), U.S. DOJ/DEA [Interagency agreement D-15-OD-0002] (AJ), Department of Veterans Affairs Merit Review [I01BX002758] and Department of Veterans Affairs Award Senior Research Career Scientist programs [1IK6BX005754] (AJ), and NIH/NIDA [Interagency agreement ADA12013] (AJ), the John F. and Nancy A. Emmerling Fund of The Pittsburgh Foundation (ZF), the NIDA Intramural Research Program Z1ADA000424 (AHN), the NIDA Medications Development Program (AHN), and the NIDA Addiction Treatment Discovery Program (ATDP). The contents do not represent the views of the U.S. Department of Veterans Affairs, U.S. Department of Justice, Drug Enforcement Administration, or the United States Government.

Conflict of interest: The authors have declared that no conflict of interest exists.

References

1. Ter Horst KW, Lammers NM, Trinko R, Opland DM, Figee M, Ackermans MT *et al.* Striatal dopamine regulates systemic glucose metabolism in humans and mice. *Sci Transl Med* 2018; **10**(442).

2. Chakravarthy S, Balasubramani PP, Mandali A, Jahanshahi M, Moustafa AA. The many facets of dopamine: Toward an integrative theory of the role of dopamine in managing the body's energy resources. *Physiol Behav* 2018; **195:** 128-141.

3. Davis LM, Michaelides M, Cheskin LJ, Moran TH, Aja S, Watkins PA *et al.* Bromocriptine administration reduces hyperphagia and adiposity and differentially affects dopamine D2 receptor and transporter binding in leptin-receptor-deficient Zucker rats and rats with diet-induced obesity. *Neuroendocrinology* 2009; **89**(2)**:** 152-162.

4. de Leeuw van Weenen JE, Parlevliet ET, Schroder-van der Elst JP, van den Berg SA, Willems van Dijk K, Romijn JA *et al.* Pharmacological modulation of dopamine receptor

D2-mediated transmission alters the metabolic phenotype of diet induced obese and diet resistant C57Bl6 mice. *Experimental diabetes research* 2011; **2011:** 928523.

5. Ezrokhi M, Luo S, Trubitsyna Y, Cincotta AH. Neuroendocrine and metabolic components of dopamine agonist amelioration of metabolic syndrome in SHR rats. *Diabetology & metabolic syndrome* 2014; **6:** 104.

6. Freyberg Z, McCarthy MJ. Dopamine D_2 receptors and the circadian clock reciprocally mediate antipsychotic drug-induced metabolic disturbances. *NPJ Schizophr* 2017; **3:** 17.

7. Kohlie R, Perwitz N, Resch J, Schmid SM, Lehnert H, Klein J *et al.* Dopamine directly increases mitochondrial mass and thermogenesis in brown adipocytes. *J Mol Endocrinol* 2017; **58**(2)**:** 57-66.

8. Palmiter RD. Is dopamine a physiologically relevant mediator of feeding behavior? *Trends Neurosci* 2007; **30**(8)**:** 375-381.

9. Simpson N, Maffei A, Freeby M, Burroughs S, Freyberg Z, Javitch J *et al.* Dopamine-mediated autocrine inhibitory circuit regulating human insulin secretion in vitro. *Mol Endocrinol* 2012; **26**(10)**:** 1757-1772.

10. Garcia-Tornadu I, Perez-Millan MI, Recouvreux V, Ramirez MC, Luque G, Risso GS *et al.* New insights into the endocrine and metabolic roles of dopamine D2 receptors gained from the Drd2 mouse. *Neuroendocrinology* 2010; **92**(4)**:** 207-214.

11. Farino ZJ, Morgenstern TJ, Maffei A, Quick M, De Solis AJ, Wiriyasermkul P *et al.* New roles for dopamine D(2) and D(3) receptors in pancreatic beta cell insulin secretion. *Mol Psychiatry* 2020; **25**(9)**:** 2070-2085.

12. Aslanoglou D, Bertera S, Friggeri L, Sánchez-Soto M, Lee J, Xue X *et al.* Dual pancreatic adrenergic and dopaminergic signaling as a therapeutic target of bromocriptine. *iScience* 2022; **25**(8)**:** 104771.

13. Aslanoglou D, Bertera S, Sánchez-Soto M, Benjamin Free R, Lee J, Zong W *et al.* Dopamine regulates pancreatic glucagon and insulin secretion via adrenergic and dopaminergic receptors. *Translational psychiatry* 2021; **11**(1)**:** 59.

14. Uvnäs-Moberg K, Ahlenius S, Alster P, Hillegaart V. Effects of selective serotonin and dopamine agonists on plasma levels of glucose, insulin and glucagon in the rat. *Neuroendocrinology* 1996; **63**(3)**:** 269-274.

15. Garcia-Tornadu I, Ornstein AM, Chamson-Reig A, Wheeler MB, Hill DJ, Arany E *et al.* Disruption of the dopamine d2 receptor impairs insulin secretion and causes glucose intolerance. *Endocrinology* 2010; **151**(4)**:** 1441-1450.

16. Roh E, Song DK, Kim MS. Emerging role of the brain in the homeostatic regulation of energy and glucose metabolism. *Exp Mol Med* 2016; **48**(3)**:** e216.

17. Kern A, Albarran-Zeckler R, Walsh HE, Smith RG. Apo-ghrelin receptor forms heteromers with DRD2 in hypothalamic neurons and is essential for anorexigenic effects of DRD2 agonism. *Neuron* 2012; **73**(2)**:** 317-332.

18. Suzuki M, Hurd YL, Sokoloff P, Schwartz JC, Sedvall G. D3 dopamine receptor mRNA is widely expressed in the human brain. *Brain Res* 1998; **779**(1-2)**:** 58-74.

19. Kim KS, Yoon YR, Lee HJ, Yoon S, Kim SY, Shin SW *et al.* Enhanced hypothalamic leptin signaling in mice lacking dopamine D2 receptors. *J Biol Chem* 2010; **285**(12)**:** 8905-8917.

20. Castellani LN, Pereira S, Kowalchuk C, Asgariroozbehani R, Singh R, Wu S *et al.* Antipsychotics impair regulation of glucose metabolism by central glucose. *Mol Psychiatry* 2022.

21. Kowalchuk C, Castellani LN, Chintoh A, Remington G, Giacca A, Hahn MK. Antipsychotics and glucose metabolism: how brain and body collide. *Am J Physiol Endocrinol Metab* 2019; **316**(1)**:** E1-e15.

22. Castellani LN, Wilkin J, Abela AR, Benarroch L, Ahasan Z, Teo C *et al.* Effects of acute olanzapine exposure on central insulin-mediated regulation of whole body fuel selection and feeding. *Psychoneuroendocrinology* 2018; **98:** 127-130.

23. Baik JH. Dopamine signaling in reward-related behaviors. *Frontiers in neural circuits* 2013; **7:** 152.

24. Stice E, Yokum S, Zald D, Dagher A. Dopamine-based reward circuitry responsivity, genetics, and overeating. *Current topics in behavioral neurosciences* 2011; **6:** 81-93.

25. Barnard ND, Noble EP, Ritchie T, Cohen J, Jenkins DJ, Turner-McGrievy G *et al.* D2 dopamine receptor Taq1A polymorphism, body weight, and dietary intake in type 2 diabetes. *Nutrition* 2009; **25**(1)**:** 58-65.

26. Freyberg Z, Aslanoglou D, Shah R, Ballon JS. Intrinsic and Antipsychotic Drug-Induced Metabolic Dysfunction in Schizophrenia. *Frontiers in neuroscience* 2017; **11:** 432.

27. Rubi B, Ljubicic S, Pournourmohammadi S, Carobbio S, Armanet M, Bartley C *et al.* Dopamine D2-like receptors are expressed in pancreatic beta cells and mediate inhibition of insulin secretion. *J Biol Chem* 2005; **280**(44)**:** 36824-36832.

28. Ustione A, Piston DW, Harris PE. Minireview: Dopaminergic regulation of insulin secretion from the pancreatic islet. *Mol Endocrinol* 2013; **27**(8)**:** 1198-1207.

29. Ustione A, Piston DW. Dopamine synthesis and D3 receptor activation in pancreatic beta-cells regulates insulin secretion and intracellular [Ca(2+)] oscillations. *Mol Endocrinol* 2012; **26**(11)**:** 1928-1940.

30. Mitok KA, Freiberger EC, Schueler KL, Rabaglia ME, Stapleton DS, Kwiecien NW *et al.* Islet proteomics reveals genetic variation in dopamine production resulting in altered insulin secretion. *J Biol Chem* 2018; **293**(16)**:** 5860-5877.

31. Hughes JW, Ustione A, Lavagnino Z, Piston DW. Regulation of islet glucagon secretion: Beyond calcium. *Diabetes, obesity & metabolism* 2018; **20 Suppl 2:** 127-136.

32. Freyberg Z, Gittes GK. Roles of Pancreatic Islet Catecholamine Neurotransmitters in Glycemic Control and in Antipsychotic Drug-Induced Dysglycemia. *Diabetes* 2023; **72**(1)**:** 3-15.

33. Smith GC, Chaussade C, Vickers M, Jensen J, Shepherd PR. Atypical antipsychotic drugs induce derangements in glucose homeostasis by acutely increasing glucagon secretion and hepatic glucose output in the rat. *Diabetologia* 2008; **51**(12)**:** 2309-2317.

34. Castellani LN, Peppler WT, Sutton CD, Whitfield J, Charron MJ, Wright DC. Glucagon receptor knockout mice are protected against acute olanzapine-induced hyperglycemia. *Psychoneuroendocrinology* 2017; **82:** 38-45.

35. Hahn M, Chintoh A, Giacca A, Xu L, Lam L, Mann S *et al.* Atypical antipsychotics and effects of muscarinic, serotonergic, dopaminergic and histaminergic receptor binding on insulin secretion in vivo: an animal model. *Schizophr Res* 2011; **131**(1-3)**:** 90-95.

36. Mehran AE, Templeman NM, Brigidi GS, Lim GE, Chu KY, Hu X *et al.* Hyperinsulinemia drives diet-induced obesity independently of brain insulin production. *Cell Metab* 2012; **16**(6)**:** 723-737.

37. Ballon JS, Pajvani U, Freyberg Z, Leibel RL, Lieberman JA. Molecular pathophysiology of metabolic effects of antipsychotic medications. *Trends in endocrinology and metabolism: TEM* 2014.

38. Lamos EM, Levitt DL, Munir KM. A review of dopamine agonist therapy in type 2 diabetes and effects on cardio-metabolic parameters. *Primary care diabetes* 2016; **10**(1)**:** 60-65.

39. Bahar A, Kashi Z, Daneshpour E, Akha O, Ala S. Effects of cabergoline on blood glucose levels in type 2 diabetic patients: A double-blind controlled clinical trial. *Medicine (Baltimore)* 2016; **95**(40).

40. Tavares G, Marques D, Barra C, Rosendo-Silva D, Costa A, Rodrigues T *et al.* Dopamine D2 receptor agonist, bromocriptine, remodels adipose tissue dopaminergic signalling and upregulates catabolic pathways, improving metabolic profile in type 2 diabetes. *Molecular metabolism* 2021; **51:** 101241.

41. Kerr JL, Timpe EM, Petkewicz KA. Bromocriptine mesylate for glycemic management in type 2 diabetes mellitus. *The Annals of pharmacotherapy* 2010; **44**(11)**:** 1777-1785.

42. Lopez Vicchi F, Luque GM, Brie B, Nogueira JP, Garcia Tornadu I, Becu-Villalobos D. Dopaminergic drugs in type 2 diabetes and glucose homeostasis. *Pharmacological research* 2016; **109:** 74-80.

43. Bahler L, Verberne HJ, Brakema E, Tepaske R, Booij J, Hoekstra JB *et al.* Bromocriptine and insulin sensitivity in lean and obese subjects. *Endocrine connections* 2016; **5**(6)**:** 44-52.

44. Shivaprasad C, Kalra S. Bromocriptine in type 2 diabetes mellitus. *Indian journal of endocrinology and metabolism* 2011; **15**(Suppl 1)**:** S17-24.

45. Benoit SC, McQuade JA, Clegg DJ, Xu M, Rushing PA, Woods SC *et al.* Altered feeding responses in mice with targeted disruption of the dopamine-3 receptor gene. *Behav Neurosci* 2003; **117**(1)**:** 46-54.

46. Diaz-Torga G, Feierstein C, Libertun C, Gelman D, Kelly MA, Low MJ *et al.* Disruption of the D2 dopamine receptor alters GH and IGF-I secretion and causes dwarfism in male mice. *Endocrinology* 2002; **143**(4)**:** 1270-1279.

47. Perez Millan MI, Luque GM, Ramirez MC, Noain D, Ornstein AM, Rubinstein M *et al.* Selective disruption of dopamine D2 receptors in pituitary lactotropes increases body weight and adiposity in female mice. *Endocrinology* 2014; **155**(3)**:** 829-839.

48. Zou MF, Keck TM, Kumar V, Donthamsetti P, Michino M, Burzynski C *et al.* Novel Analogues of (R)-5-(Methylamino)-5,6-dihydro-4H-imidazo[4,5,1-ij]quinolin-2(1H)-one (Sumanirole) Provide Clues to Dopamine D2/D3 Receptor Agonist Selectivity. *Journal of medicinal chemistry* 2016; **59**(7)**:** 2973-2988.

49. Bonifazi A, Yano H, Ellenberger MP, Muller L, Kumar V, Zou MF *et al.* Novel Bivalent Ligands Based on the Sumanirole Pharmacophore Reveal Dopamine D2 Receptor (D2R) Biased Agonism. *Journal of medicinal chemistry* 2017; **60**(7)**:** 2890-2907.

50. Kulagowski JJ, Broughton HB, Curtis NR, Mawer IM, Ridgill MP, Baker R *et al.* 3-((4-(4-Chlorophenyl)piperazin-1-yl)-methyl)-1H-pyrrolo-2,3-b-pyridine: an antagonist with high affinity and selectivity for the human dopamine D4 receptor. *Journal of medicinal chemistry* 1996; **39**(10)**:** 1941-1942.

51. Keck TM, Free RB, Day MM, Brown SL, Maddaluna MS, Fountain G *et al.* Dopamine D(4) Receptor-Selective Compounds Reveal Structure-Activity Relationships that Engender Agonist Efficacy. *Journal of medicinal chemistry* 2019; **62**(7)**:** 3722-3740.

52. Cheng Y, Prusoff WH. Relationship between the inhibition constant (K1) and the concentration of inhibitor which causes 50 per cent inhibition (I50) of an enzymatic reaction. *Biochemical pharmacology* 1973; **22**(23)**:** 3099-3108.

53. Galaj E, Bi GH, Klein B, Hempel B, Shaik AB, Gogarnoiu ES *et al.* A highly D(3)R-selective and efficacious partial agonist (S)-ABS01-113 compared to its D(3)R-selective antagonist enantiomer (R)-ABS01-113 as potential treatments for opioid use disorder. *Neuropsychopharmacology* 2022; **47**(13)**:** 2309-2318.

54. Janowsky A, Eshleman AJ, Johnson RA, Wolfrum KM, Hinrichs DJ, Yang J *et al.* Mefloquine and psychotomimetics share neurotransmitter receptor and transporter interactions in vitro. *Psychopharmacology (Berl)* 2014; **231**(14)**:** 2771-2783.

55. Merglen A, Theander S, Rubi B, Chaffard G, Wollheim CB, Maechler P. Glucose sensitivity and metabolism-secretion coupling studied during two-year continuous culture in INS-1E insulinoma cells. *Endocrinology* 2004; **145**(2)**:** 667-678.

56. Farino ZJ, Morgenstern TJ, Vallaghe J, Gregor N, Donthamsetti P, Harris PE *et al.* Development of a Rapid Insulin Assay by Homogenous Time-Resolved Fluorescence. *PLoS One* 2016; **11**(2)**:** e0148684.

57. Aslanoglou D, George EW, Freyberg Z. Homogeneous Time-resolved Forster Resonance Energy Transfer-based Assay for Detection of Insulin Secretion. *J Vis Exp* 2018; (135).

58. Knight AR, Misra A, Quirk K, Benwell K, Revell D, Kennett G *et al.* Pharmacological characterisation of the agonist radioligand binding site of 5-HT(2A), 5-HT(2B) and 5-HT(2C) receptors. *Naunyn Schmiedebergs Arch Pharmacol* 2004; **370**(2)**:** 114-123.

59. Eshleman AJ, Carmolli M, Cumbay M, Martens CR, Neve KA, Janowsky A. Characteristics of drug interactions with recombinant biogenic amine transporters expressed in the same cell type. *J Pharmacol Exp Ther* 1999; **289**(2)**:** 877-885.

60. Bonaventura J, Eldridge MAG, Hu F, Gomez JL, Sanchez-Soto M, Abramyan AM *et al.* High-potency ligands for DREADD imaging and activation in rodents and monkeys. *Nature communications* 2019; **10**(1)**:** 4627.

61. Ku TC, Cao J, Won SJ, Guo J, Camacho-Hernandez GA, Okorom AV *et al.* Series of (([1,1′-Biphenyl]-2-yl)methyl)sulfinylalkyl Alicyclic Amines as Novel and High Affinity Atypical Dopamine Transporter Inhibitors with Reduced hERG Activity. *ACS pharmacology & translational science* 2024.

62. Mathes C. QPatch: the past, present and future of automated patch clamp. *Expert opinion on therapeutic targets* 2006; **10**(2)**:** 319-327.

63. Zou MF, Cao J, Abramyan AM, Kopajtic T, Zanettini C, Guthrie DA *et al.* Structure-Activity Relationship Studies on a Series of 3α-[Bis(4-fluorophenyl)methoxy]tropanes and 3α-[Bis(4-fluorophenyl)methylamino]tropanes As Novel Atypical Dopamine Transporter (DAT) Inhibitors for the Treatment of Cocaine Use Disorders. *Journal of medicinal chemistry* 2017; **60**(24)**:** 10172-10187.

64. Kilkenny C, Browne W, Cuthill IC, Emerson M, Altman DG. Animal research: reporting in vivo experiments: the ARRIVE guidelines. *The journal of gene medicine* 2010; **12**(7)**:** 561-563.

65. Kilkenny C, Browne WJ, Cuthill IC, Emerson M, Altman DG. Improving bioscience research reporting: the ARRIVE guidelines for reporting animal research. *PLoS Biol* 2010; **8**(6)**:** e1000412.

66. Hrovatin K, Bastidas-Ponce A, Bakhti M, Zappia L, Büttner M, Salinno C *et al.* Delineating mouse β-cell identity during lifetime and in diabetes with a single cell atlas. *Nature metabolism* 2023; **5**(9)**:** 1615-1637.

67. Yong HJ, Toledo MP, Nowakowski RS, Wang YJ. Sex Differences in the Molecular Programs of Pancreatic Cells Contribute to the Differential Risks of Type 2 Diabetes. *Endocrinology* 2022; **163**(11).

68. Berhane I, Hin N, Thomas AG, Huang Q, Zhang C, Veeravalli V *et al.* Thieno[2,3-d]pyrimidine-Based Positive Allosteric Modulators of Human Mas-Related G Protein-Coupled Receptor X1 (MRGPRX1). *Journal of medicinal chemistry* 2022; **65**(4)**:** 3218-3228.

69. Tunstall BJ, Ho CP, Cao J, Vendruscolo JCM, Schmeichel BE, Slack RD *et al.* Atypical dopamine transporter inhibitors attenuate compulsive-like methamphetamine self-administration in rats. *Neuropharmacology* 2018; **131:** 96-103.

70. Rojas C, Sala M, Thomas AG, Datta Chaudhuri A, Yoo SW, Li Z *et al.* A novel and potent brain penetrant inhibitor of extracellular vesicle release. *British journal of pharmacology* 2019; **176**(19)**:** 3857-3870.

71. Ezrokhi M, Zhang Y, Luo S, Cincotta AH. Time-of-Day-Dependent Effects of Bromocriptine to Ameliorate Vascular Pathology and Metabolic Syndrome in SHR Rats Held on High Fat Diet. *International journal of molecular sciences* 2021; **22**(11).

72. Hansen HH, Perens J, Roostalu U, Skytte JL, Salinas CG, Barkholt P *et al.* Whole-brain activation signatures of weight-lowering drugs. *Molecular metabolism* 2021; **47:** 101171.

73. Hintze KJ, Benninghoff AD, Cho CE, Ward RE. Modeling the Western Diet for Preclinical Investigations. *Advances in nutrition (Bethesda, Md)* 2018; **9**(3)**:** 263-271.

74. Zheng X, Li Z, Berg Sen J, Samarah L, Deacon CS, Bernardo J *et al.* Western diet augments metabolic and arterial dysfunction in a sex-specific manner in outbred, genetically diverse mice. *Front Nutr* 2022; **9:** 1090023.

75. Marcelin G, Jo YH, Li X, Schwartz GJ, Zhang Y, Dun NJ *et al.* Central action of FGF19 reduces hypothalamic AGRP/NPY neuron activity and improves glucose metabolism. *Molecular metabolism* 2014; **3**(1)**:** 19-28.

76. Kowalchuk C, Teo C, Wilson V, Chintoh A, Lam L, Agarwal SM *et al.* In male rats, the ability of central insulin to suppress glucose production is impaired by olanzapine, whereas glucose uptake is left intact. *J Psychiatry Neurosci* 2017; **42**(6)**:** 424-431.

77. Hill ER, Tian J, Tilley MR, Zhu MX, Gu HH. Potencies of cocaine methiodide on major cocaine targets in mice. *PLoS One* 2009; **4**(10)**:** e7578.

78. Lewanowitsch T, Irvine RJ. Naloxone methiodide reverses opioid-induced respiratory depression and analgesia without withdrawal. *Eur J Pharmacol* 2002; **445**(1-2)**:** 61-67.

79. Schindler CW, Tella SR, Katz JL, Goldberg SR. Effects of cocaine and its quaternary derivative cocaine methiodide on cardiovascular function in squirrel monkeys. *Eur J Pharmacol* 1992; **213**(1)**:** 99-105.

80. Aceto MD, Awaya H, Martin BR, May EL. Antinociceptive action of nicotine and its methiodide derivatives in mice and rats. *British journal of pharmacology* 1983; **79**(4)**:** 869-876.

81. Wood M, Reavill C. Aripiprazole acts as a selective dopamine D2 receptor partial agonist. *Expert opinion on investigational drugs* 2007; **16**(6)**:** 771-775.

82. Yokoi F, Gründer G, Biziere K, Stephane M, Dogan AS, Dannals RF *et al.* Dopamine D2 and D3 receptor occupancy in normal humans treated with the antipsychotic drug aripiprazole (OPC 14597): a study using positron emission tomography and [11C]raclopride. *Neuropsychopharmacology* 2002; **27**(2)**:** 248-259.

83. Foust DJP, Ustione A, Piston DW. Fluorescence Fluctuation Spectroscopy of Dopaminergic Signaling in Pancreatic Beta Cells. *Biophysical Journal* 2017; **112**(3)**:** 89a.

84. Farino ZJ, Morgenstern TJ, Maffei A, Quick M, De Solis AJ, Wiriyasermkul P *et al.* New roles for dopamine D2 and D3 receptors in pancreatic beta cell insulin secretion. *Mol Psychiatry* 2019.

85. McCall RB, Lookingland KJ, Bédard PJ, Huff RM. Sumanirole, a highly dopamine D2-selective receptor agonist: in vitro and in vivo pharmacological characterization and efficacy in animal models of Parkinson's disease. *J Pharmacol Exp Ther* 2005; **314**(3)**:** 1248-1256.

86. Millan MJ, Girardon S, Monneyron S, Dekeyne A. Discriminative stimulus properties of the dopamine D3 receptor agonists, PD128,907 and 7-OH-DPAT: a comparative characterization with novel ligands at D3 versus D2 receptors. *Neuropharmacology* 2000; **39**(4)**:** 586-598.

87. Zhu L, Almaca J, Dadi PK, Hong H, Sakamoto W, Rossi M *et al.* beta-arrestin-2 is an essential regulator of pancreatic beta-cell function under physiological and pathophysiological conditions. *Nature communications* 2017; **8:** 14295.

88. Masri B, Salahpour A, Didriksen M, Ghisi V, Beaulieu JM, Gainetdinov RR *et al.* Antagonism of dopamine D2 receptor/beta-arrestin 2 interaction is a common property of clinically effective antipsychotics. *Proc Natl Acad Sci U S A* 2008; **105**(36)**:** 13656-13661.

89. Beaulieu JM, Espinoza S, Gainetdinov RR. Dopamine receptors - IUPHAR Review 13. *British journal of pharmacology* 2015; **172**(1)**:** 1-23.

90. Machleidt T, Woodroofe CC, Schwinn MK, Mendez J, Robers MB, Zimmerman K *et al.* NanoBRET--A Novel BRET Platform for the Analysis of Protein-Protein Interactions. *ACS Chem Biol* 2015; **10**(8)**:** 1797-1804.

91. Zawilska J, Iuvone PM. Alpha-2 adrenergic activity of bromocriptine and quinpirole in chicken pineal gland. Effects on melatonin synthesis and [3H]rauwolscine binding. *J Pharmacol Exp Ther* 1990; **255**(3)**:** 1047-1052.

92. de Leeuw van Weenen JE, Parlevliet ET, Maechler P, Havekes LM, Romijn JA, Ouwens DM *et al.* The dopamine receptor D2 agonist bromocriptine inhibits glucose-stimulated

insulin secretion by direct activation of the alpha2-adrenergic receptors in beta cells. *Biochemical pharmacology* 2010; **79**(12)**:** 1827-1836.

93. Patil VM, Gaurav A, Garg P, Masand N. Non-cancer to anti-cancer: investigation of human ether-a-go-go-related gene potassium channel inhibitors as potential therapeutics. *J Egypt Natl Canc Inst* 2021; **33**(1)**:** 33.

94. Cincotta AH, Schiller BC, Meier AH. Bromocriptine inhibits the seasonally occurring obesity, hyperinsulinemia, insulin resistance, and impaired glucose tolerance in the Syrian hamster, Mesocricetus auratus. *Metabolism: clinical and experimental* 1991; **40**(6)**:** 639-644.

95. Defronzo RA. Bromocriptine: a sympatholytic, d2-dopamine agonist for the treatment of type 2 diabetes. *Diabetes Care* 2011; **34**(4)**:** 789-794.

96. Prevention CfDCa. National Diabetes Statistics Report, 2017. Atlanta, GA: Centers for Disease Control and Prevention, U.S. Dept of Health and Human Services; 2017.

97. Meloni A, Cadeddu C, Cugusi L, Donataccio MP, Deidda M, Sciomer S *et al.* Gender Differences and Cardiometabolic Risk: The Importance of the Risk Factors. *International journal of molecular sciences* 2023; **24**(2).

98. Scirica BM. Use of Biomarkers in Predicting the Onset, Monitoring the Progression, and Risk Stratification for Patients with Type 2 Diabetes Mellitus. *Clinical chemistry* 2017; **63**(1)**:** 186-195.

99. Moore TJ, Mattison DR. Adult Utilization of Psychiatric Drugs and Differences by Sex, Age, and Race. *JAMA internal medicine* 2017; **177**(2)**:** 274-275.

100. Alexander GC, Gallagher SA, Mascola A, Moloney RM, Stafford RS. Increasing off-label use of antipsychotic medications in the United States, 1995-2008. *Pharmacoepidemiology and drug safety* 2011; **20**(2)**:** 177-184.

101. Freedman R. Schizophrenia. *N Engl J Med* 2003; **349**(18)**:** 1738-1749.

102. Newcomer JW. Metabolic considerations in the use of antipsychotic medications: a review of recent evidence. *J Clin Psychiatry* 2007; **68 Suppl 1:** 20-27.

103. Fleischhacker WW, Siu CO, Boden R, Pappadopulos E, Karayal ON, Kahn RS *et al.* Metabolic risk factors in first-episode schizophrenia: baseline prevalence and course analysed from the European First-Episode Schizophrenia Trial. *Int J Neuropsychopharmacol* 2012**:** 1-9.

104. Gordon HL, Law A, Hohman KE, Groth C. The problem of overweight in hospitalized psychotic patients. *The Psychiatric quarterly* 1960; **34:** 69-82.

105. Spertus J, Horvitz-Lennon M, Abing H, Normand SL. Risk of weight gain for specific antipsychotic drugs: a meta-analysis. *NPJ Schizophr* 2018; **4**(1)**:** 12.

106. Adams CE, Awad GA, Rathbone J, Thornley B, Soares-Weiser K. Chlorpromazine versus placebo for schizophrenia. *The Cochrane database of systematic reviews* 2014; (1)**:** Cd000284.

107. Karam CS, Ballon JS, Bivens NM, Freyberg Z, Girgis RR, Lizardi-Ortiz JE *et al.* Signaling pathways in schizophrenia: emerging targets and therapeutic strategies. *Trends Pharmacol Sci* 2010; **31**(8)**:** 381-390.

108. Freyberg Z, McCarthy MJ. Dopamine D2 receptors and the circadian clock reciprocally mediate antipsychotic drug-induced metabolic disturbances. *npj Schizophrenia* 2017; **3**(1)**:** 17.

109. Kroeze WK, Hufeisen SJ, Popadak BA, Renock SM, Steinberg S, Ernsberger P *et al.* H1-histamine receptor affinity predicts short-term weight gain for typical and atypical antipsychotic drugs. *Neuropsychopharmacology* 2003; **28**(3)**:** 519-526.

110. Mahajan R. Bromocriptine mesylate: FDA-approved novel treatment for type-2 diabetes. *Indian journal of pharmacology* 2009; **41**(4)**:** 197-198.

111. Beaulieu JM, Gainetdinov RR. The physiology, signaling, and pharmacology of dopamine receptors. *Pharmacol Rev* 2011; **63**(1)**:** 182-217.

112. Meguid MM, Fetissov SO, Varma M, Sato T, Zhang L, Laviano A *et al.* Hypothalamic dopamine and serotonin in the regulation of food intake. *Nutrition* 2000; **16**(10)**:** 843-857.

113. Wang GJ, Volkow ND, Fowler JS. The role of dopamine in motivation for food in humans: implications for obesity. *Expert opinion on therapeutic targets* 2002; **6**(5)**:** 601-609.

114. Morutto SL, Phillips GD. Post-session intra-perifornical region quinpirole infusions retard the consolidation of an appetitive differential conditioning task. *Behavioural pharmacology* 1999; **10**(1)**:** 113-118.

115. Vucetic Z, Reyes TM. Central dopaminergic circuitry controlling food intake and reward: implications for the regulation of obesity. *Wiley Interdiscip Rev Syst Biol Med* 2010; **2**(5)**:** 577-593.

116. Gross G, Drescher K. The role of dopamine D(3) receptors in antipsychotic activity and cognitive functions. *Handb Exp Pharmacol* 2012; (213)**:** 167-210.

117. Pirchio R, Graziadio C, Colao A, Pivonello R, Auriemma RS. Metabolic effects of prolactin. *Frontiers in endocrinology* 2022; **13:** 1015520.

118. Luque GM, Lopez-Vicchi F, Ornstein AM, Brie B, De Winne C, Fiore E *et al.* Chronic hyperprolactinemia evoked by disruption of lactotrope dopamine D2 receptors impacts on liver and adipocyte genes related to glucose and insulin balance. *Am J Physiol Endocrinol Metab* 2016; **311**(6)**:** E974-e988.

119. Narayanan NS, Guarnieri DJ, DiLeone RJ. Metabolic hormones, dopamine circuits, and feeding. *Frontiers in neuroendocrinology* 2010; **31**(1)**:** 104-112.

120. Geisler CE, Hayes MR. Metabolic hormone action in the VTA: Reward-directed behavior and mechanistic insights. *Physiology & behavior* 2023; **268:** 114236.

121. Lisco G, De Tullio A, Iovino M, Disoteo O, Guastamacchia E, Giagulli VA *et al.* Dopamine in the Regulation of Glucose Homeostasis, Pathogenesis of Type 2 Diabetes, and Chronic Conditions of Impaired Dopamine Activity/Metabolism: Implication for Pathophysiological and Therapeutic Purposes. *Biomedicines* 2023; **11**(11).

122. LeSauter J, Balsam PD, Simpson EH, Silver R. Overexpression of striatal D2 receptors reduces motivation thereby decreasing food anticipatory activity. *The European journal of neuroscience* 2020; **51**(1)**:** 71-81.

123. Halpern CH, Tekriwal A, Santollo J, Keating JG, Wolf JA, Daniels D *et al.* Amelioration of binge eating by nucleus accumbens shell deep brain stimulation in mice involves D2 receptor modulation. *J Neurosci* 2013; **33**(17)**:** 7122-7129.

124. Johnson PM, Kenny PJ. Dopamine D2 receptors in addiction-like reward dysfunction and compulsive eating in obese rats. *Nat Neurosci* 2010; **13**(5)**:** 635-641.

125. Mizuno Y, Suzuki T, Nakagawa A, Yoshida K, Mimura M, Fleischhacker WW *et al.* Pharmacological strategies to counteract antipsychotic-induced weight gain and metabolic adverse effects in schizophrenia: a systematic review and meta-analysis. *Schizophr Bull* 2014; **40**(6)**:** 1385-1403.

126. Teff KL, Rickels MR, Grudziak J, Fuller C, Nguyen HL, Rickels K. Antipsychotic-induced insulin resistance and postprandial hormonal dysregulation independent of weight gain or psychiatric disease. *Diabetes* 2013; **62**(9)**:** 3232-3240.

127. Hahn MK, Wolever TM, Arenovich T, Teo C, Giacca A, Powell V *et al.* Acute effects of single-dose olanzapine on metabolic, endocrine, and inflammatory markers in healthy controls. *Journal of clinical psychopharmacology* 2013; **33**(6)**:** 740-746.

128. Nakasone T, Wakuda H, Sugimoto Y, Kamei C. Effects of ICI204,448, naloxone methiodide and levocetirizine on the scratching behavior induced by a kappa-opioid antagonist, nor-BNI, in ICR mice. *Immunopharmacol Immunotoxicol* 2017; **39**(5)**:** 292-295.

129. Wang B, You Z-B, Oleson EB, Cheer JF, Myal S, Wise RA. Conditioned Contribution of Peripheral Cocaine Actions to Cocaine Reward and Cocaine-Seeking. *Neuropsychopharmacology* 2013; **38**(9)**:** 1763.

130. Lewanowitsch T, Miller JH, Irvine RJ. Reversal of morphine, methadone and heroin induced effects in mice by naloxone methiodide. *Life Sci* 2006; **78**(7)**:** 682-688.

131. Rosengren AH, Jokubka R, Tojjar D, Granhall C, Hansson O, Li DQ *et al.* Overexpression of alpha2A-adrenergic receptors contributes to type 2 diabetes. *Science* 2010; **327**(5962)**:** 217-220.

132. Cataldo Bascuñan LR, Lyons C, Bennet H, Artner I, Fex M. Serotonergic regulation of insulin secretion. *Acta Physiol (Oxf)* 2019; **225**(1)**:** e13101.

133. Almaca J, Molina J, Menegaz D, Pronin AN, Tamayo A, Slepak V *et al.* Human Beta Cells Produce and Release Serotonin to Inhibit Glucagon Secretion from Alpha Cells. *Cell reports* 2016; **17**(12)**:** 3281-3291.

134. Barnett AH, Chapman C, Gailer K, Hayter CJ. Effect of bromocriptine on maturity onset diabetes. *Postgrad Med J* 1980; **56**(651)**:** 11-14.

135. Lancranjan I. The endocrine profile of bromocriptine: its application in endocrine diseases. *J Neural Transm* 1981; **51**(1-2)**:** 61-82.

136. Pijl H, Ohashi S, Matsuda M, Miyazaki Y, Mahankali A, Kumar V *et al.* Bromocriptine: a novel approach to the treatment of type 2 diabetes. *Diabetes Care* 2000; **23**(8)**:** 1154-1161.

137. Valiquette G. Bromocriptine for diabetes mellitus type II. *Cardiol Rev* 2011; **19**(6)**:** 272-275.

138. Mukherjee R, Yun JW. Bromocriptine inhibits adipogenesis and lipogenesis by agonistic action on α2-adrenergic receptor in 3T3-L1 adipocyte cells. *Molecular biology reports* 2013; **40**(5)**:** 3783-3792.

139. Borcherding DC, Hugo ER, Idelman G, De Silva A, Richtand NW, Loftus J *et al.* Dopamine receptors in human adipocytes: expression and functions. *PLoS One* 2011; **6**(9)**:** e25537.

140. Wang X, Villar VA, Tiu A, Upadhyay KK, Cuevas S. Dopamine D2 receptor upregulates leptin and IL-6 in adipocytes. *J Lipid Res* 2018; **59**(4)**:** 607-614.

141. Seoane-Collazo P, Ferno J, Gonzalez F, Dieguez C, Leis R, Nogueiras R *et al.* Hypothalamic-autonomic control of energy homeostasis. *Endocrine* 2015; **50**(2)**:** 276-291.

142. Kalsbeek A, Bruinstroop E, Yi CX, Klieverik LP, La Fleur SE, Fliers E. Hypothalamic control of energy metabolism via the autonomic nervous system. *Ann N Y Acad Sci* 2010; **1212:** 114-129.

143. Shimazu T. Central nervous system regulation of liver and adipose tissue metabolism. *Diabetologia* 1981; **20**(Suppl 1)**:** 343-356.

144. Cincotta AH, Meier AH. Bromocriptine inhibits in vivo free fatty acid oxidation and hepatic glucose output in seasonally obese hamsters (Mesocricetus auratus). *Metabolism* 1995; **44**(10)**:** 1349-1355.

145. Preitner F, Mody N, Graham TE, Peroni OD, Kahn BB. Long-term Fenretinide treatment prevents high-fat diet-induced obesity, insulin resistance, and hepatic steatosis. *Am J Physiol Endocrinol Metab* 2009; **297**(6)**:** E1420-1429.

146. Chan E, Swaminathan R. Role of prolactin in lactation-induced changes in brown adipose tissue. *Am J Physiol* 1990; **258**(1 Pt 2)**:** R51-56.

147. Wei H, Zapata RC, Lopez-Valencia M, Aslanoglou D, Farino ZJ, Benner V *et al.* Dopamine D(2) receptor signaling modulates pancreatic beta cell circadian rhythms. *Psychoneuroendocrinology* 2020; **113:** 104551.

148. Stoelzel CR, Zhang Y, Cincotta AH. Circadian-timed dopamine agonist treatment reverses high-fat diet-induced diabetogenic shift in ventromedial hypothalamic glucose sensing. *Endocrinol Diabetes Metab* 2020; **3**(3)**:** e00139.

149. Petrenko V, Gandasi NR, Sage D, Tengholm A, Barg S, Dibner C. In pancreatic islets from type 2 diabetes patients, the dampened circadian oscillators lead to reduced insulin and glucagon exocytosis. *Proc Natl Acad Sci U S A* 2020; **117**(5)**:** 2484-2495.

150. Rutter J, Reick M, McKnight SL. Metabolism and the control of circadian rhythms. *Annu Rev Biochem* 2002; **71:** 307-331.

151. Prestwood TR, Asgariroozbehani R, Wu S, Agarwal SM, Logan RW, Ballon JS *et al.* Roles of inflammation in intrinsic pathophysiology and antipsychotic drug-induced metabolic disturbances of schizophrenia. *Behav Brain Res* 2021; **402:** 113101.

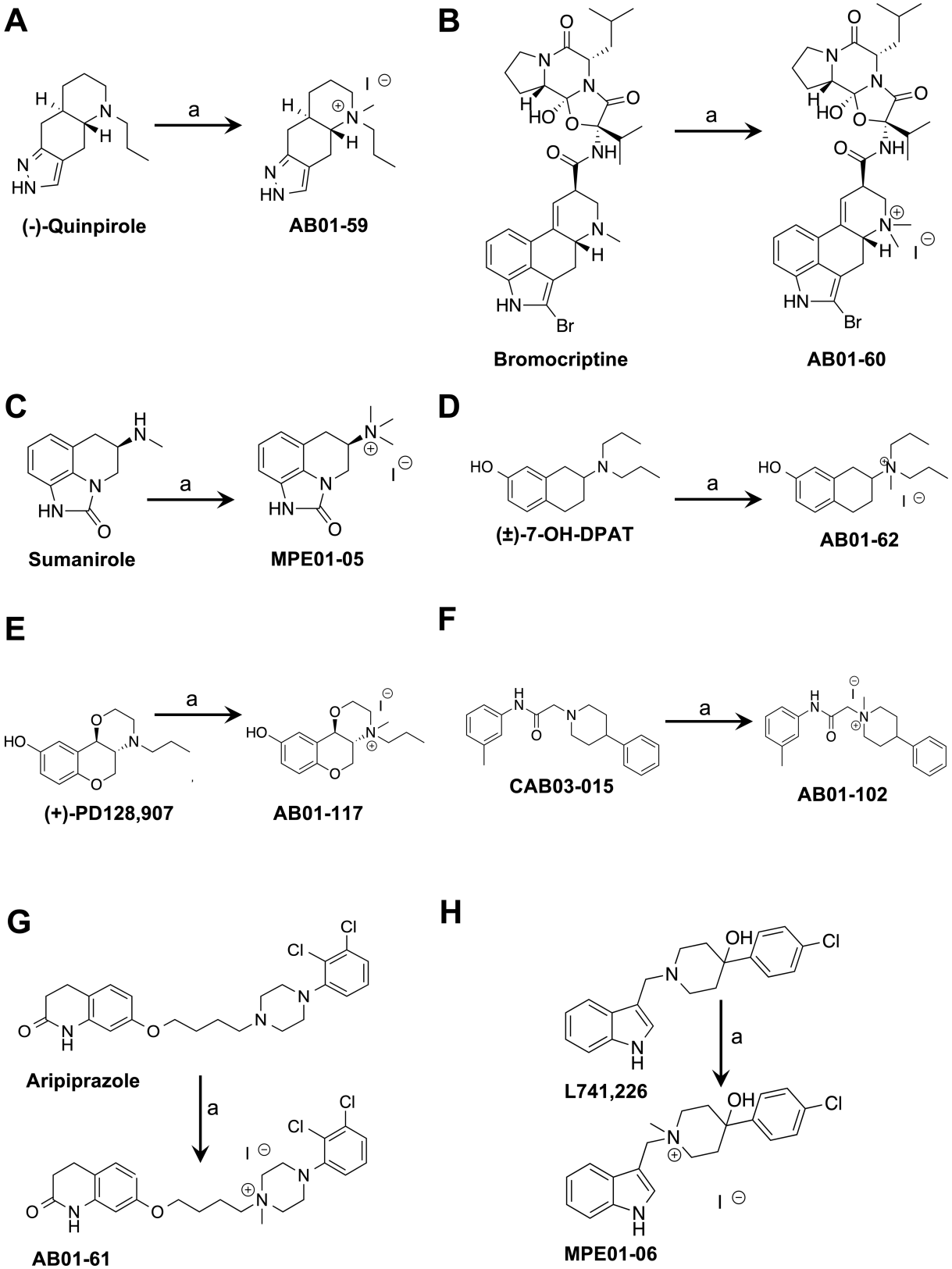

Figure 1. Drug design schemes of quaternary methiodide analogues of dopamine D_2-like receptor-targeted drugs. To selectively manipulate dopamine D_2-like receptor signaling in the periphery, drugs that target dopamine D_2-like receptors were modified via addition of a quaternary methiodide (MeI) group to render them less permeable to the blood brain barrier. These MeI analogues are based on D_2-like receptor agonists that preferentially target one or more of the receptors **(A-F)**: AB01-59 (**A**, (-)-quinpirole MeI), AB01-60 (**B**, bromocriptine MeI), MPE01-05 (**C**, sumanirole MeI), AB01-62 (**D**, (±)-7-OH-DPAT MeI), AB-01-117 (**E**, (+)-PD128,907 MeI), AB01-102 (**F**, CAB03-015 MeI); **(G)** a D_2-like receptor partial agonist: AB01-61 (aripiprazole MeI); and **(H)** a D_2-like receptor antagonist: MPE01-06 (L741,226 MeI). a = CH_3I, acetone or EtOH, 24h.

D2R

D3R

A

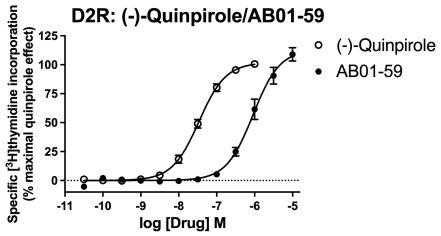

B

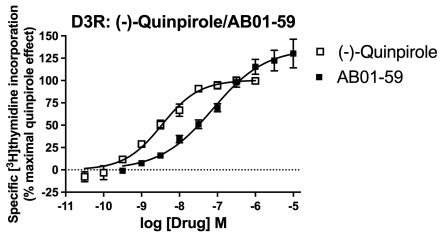

C

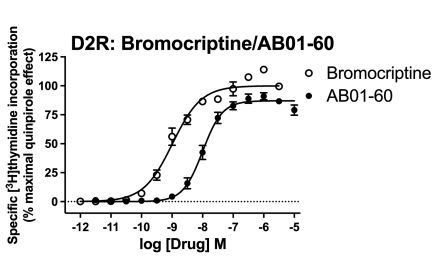

D

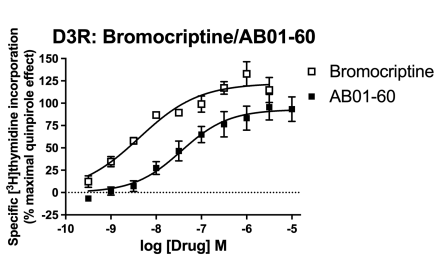

E

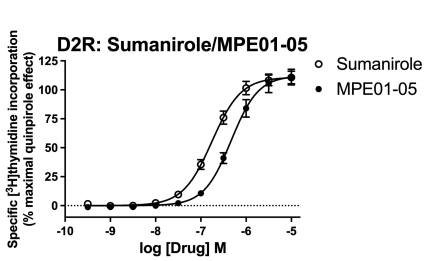

F

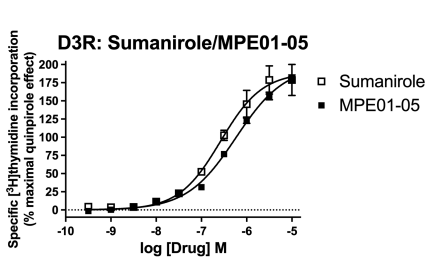

G

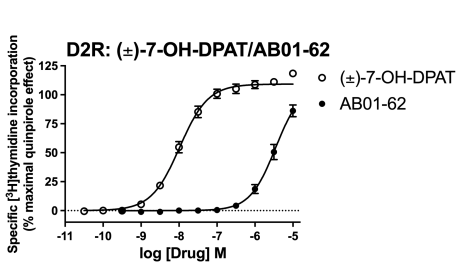

H

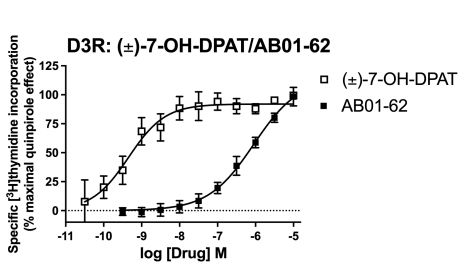

I

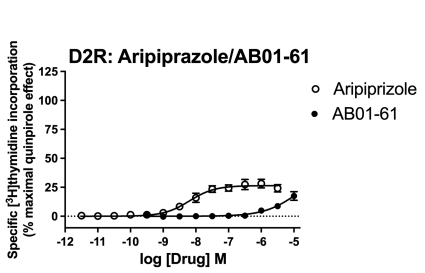

J

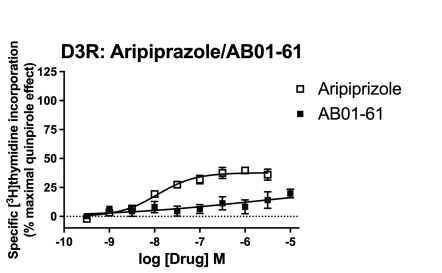

K

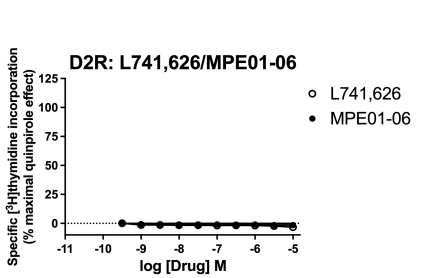

L

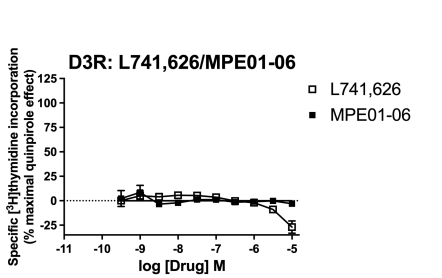

Figure 2. Impact of quaternary methiodide analogues of dopamine D_2-like receptor-targeted drugs on D2R- and D3R-mediated mitogenesis. Dose response curves demonstrating the impact of dopamine D_2-like receptor-selective drugs (open circles or squares) and their quaternary methiodide (MeI) analogues (solid circles or squares) on mitogenesis in cultured CHO cells expressing human D2R **(A, C, E, G, I, K)** or human D3R **(B, D, F, H, J, L)**. Mitogenesis was assessed according to [^{3}H]thymidine incorporation. **(A-H)** All canonical D2R/D3R agonists including (-)-quinpirole **(A, B)**, bromocriptine **(C, D)**, sumanirole **(E, F)**, (±)-7-OH-DPAT **(G, H)**, and their respective MeI analogues showed dose-dependent stimulation of D2R- and D3R-mediated mitogenesis. Compared to their unmodified parent drugs, MeI-modified agonist analogues possessed similar efficacies but diminished potencies. **(I, J)** D2R/D3R partial agonist aripiprazole exhibited decreased efficacy for both D2R- and D3R-mediated mitogenesis stimulation compared to full agonists (**A-H**). MeI analogue AB01-61 showed almost total loss of efficacy and potency versus its unmodified parent compound. **(K, L)** D2R/D3R antagonist L741,626 and its MeI analogue MPE01-06 had no effect on D2R- and D3R-mediated mitogenesis. Results for [^{3}H]thymidine incorporation for each drug were normalized to % maximal quinpirole effect. Data are represented as means ± SEM for all experimental replicates and were performed in triplicate from n ≥ 3 independent experiments.

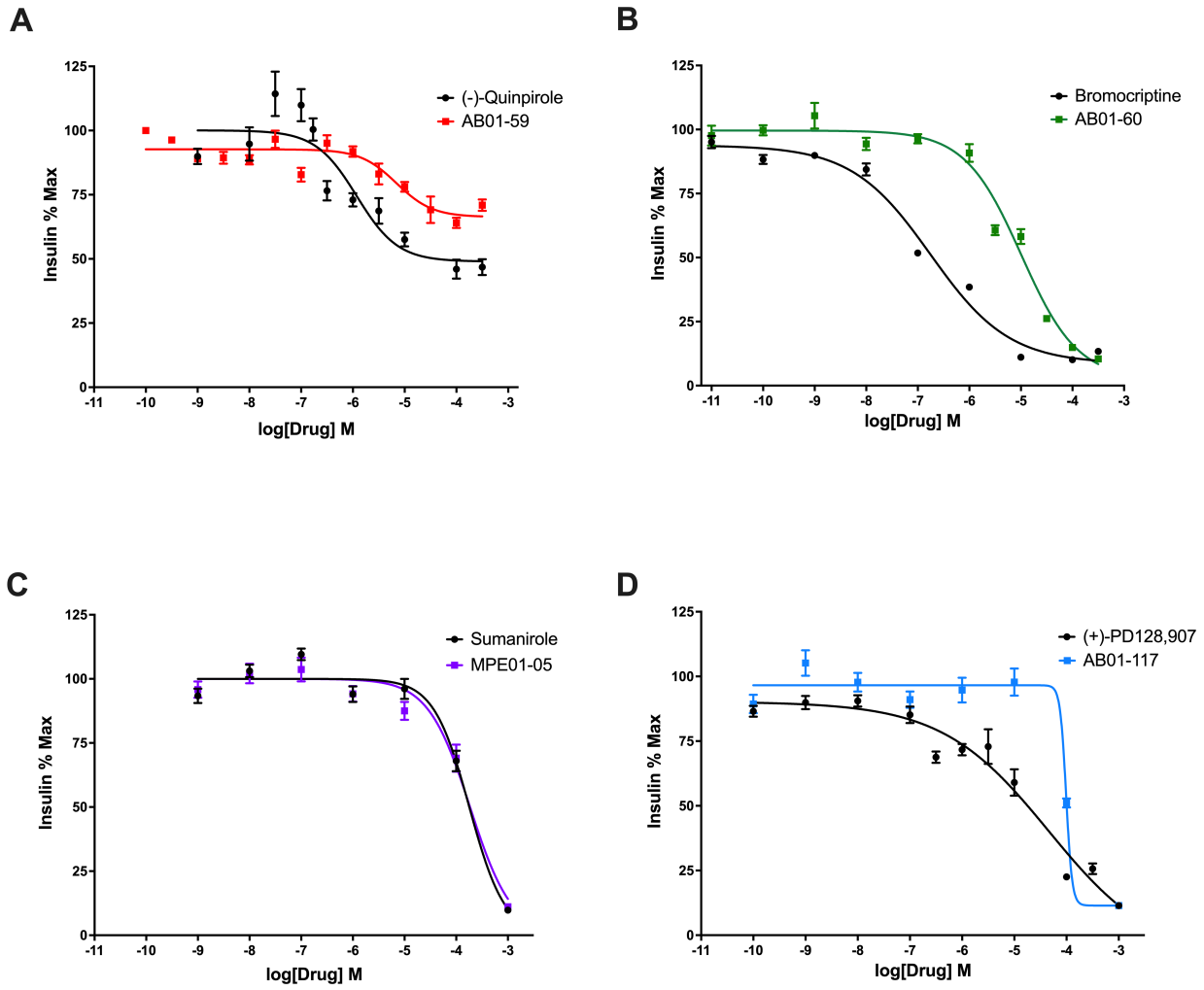

Figure 3. Impact of quaternary methiodide analogues on glucose-stimulated insulin secretion. Dose response curves demonstrating the impact of dopamine D_2-like receptor-selective drugs (circles) and their quaternary methiodide (MeI) analogues (squares) on glucose-stimulated insulin secretion (GSIS) in INS-1E cells. **(A)** Treatment with D2R/D3R agonist (-)-quinpirole produced a dose-dependent reduction of GSIS (IC_{50} = 1.18 μM). (-)-Quinpirole MeI analogue AB01-59 also decreased GSIS with reduced efficacy (48.4% decrease) and potency (IC_{50} = 6.94 μM). **(B)** Bromocriptine was more potent than (-)-quinpirole in reducing GSIS (IC_{50}=0.18 μM). Bromocriptine MeI analogue AB01-60 retained its efficacy but demonstrated decreased potency (IC_{50} = 10.17 μM) versus unmodified bromocriptine. **(C)** Selective D2R agonist sumanirole dose-dependently decreased GSIS with lower efficacy and potency (IC_{50}=17.92 μM)

than (-)-quinpirole or bromocriptine. Sumanirole MeI analogue MPE01-05 possessed nearly the same efficacy and similar potency (IC_{50}=18.50 μM) as unmodified sumanirole. **(D)** Selective D3R agonist (+)-PD128,907 produced less potent (IC_{50} = 45.43 μM) GSIS reduction compared to drugs acting via selective D2R agonism or joint D2R/D3R agonism. (+)-PD128,907 MeI analogue AB01-117 was less potent (IC_{50} = 98.19 μM) but similarly efficacious as its unmodified parent. Insulin data were normalized to % maximal secreted insulin. Data are represented as means for all experimental replicates ± SEM and were from n ≥ 2 independent experiments.

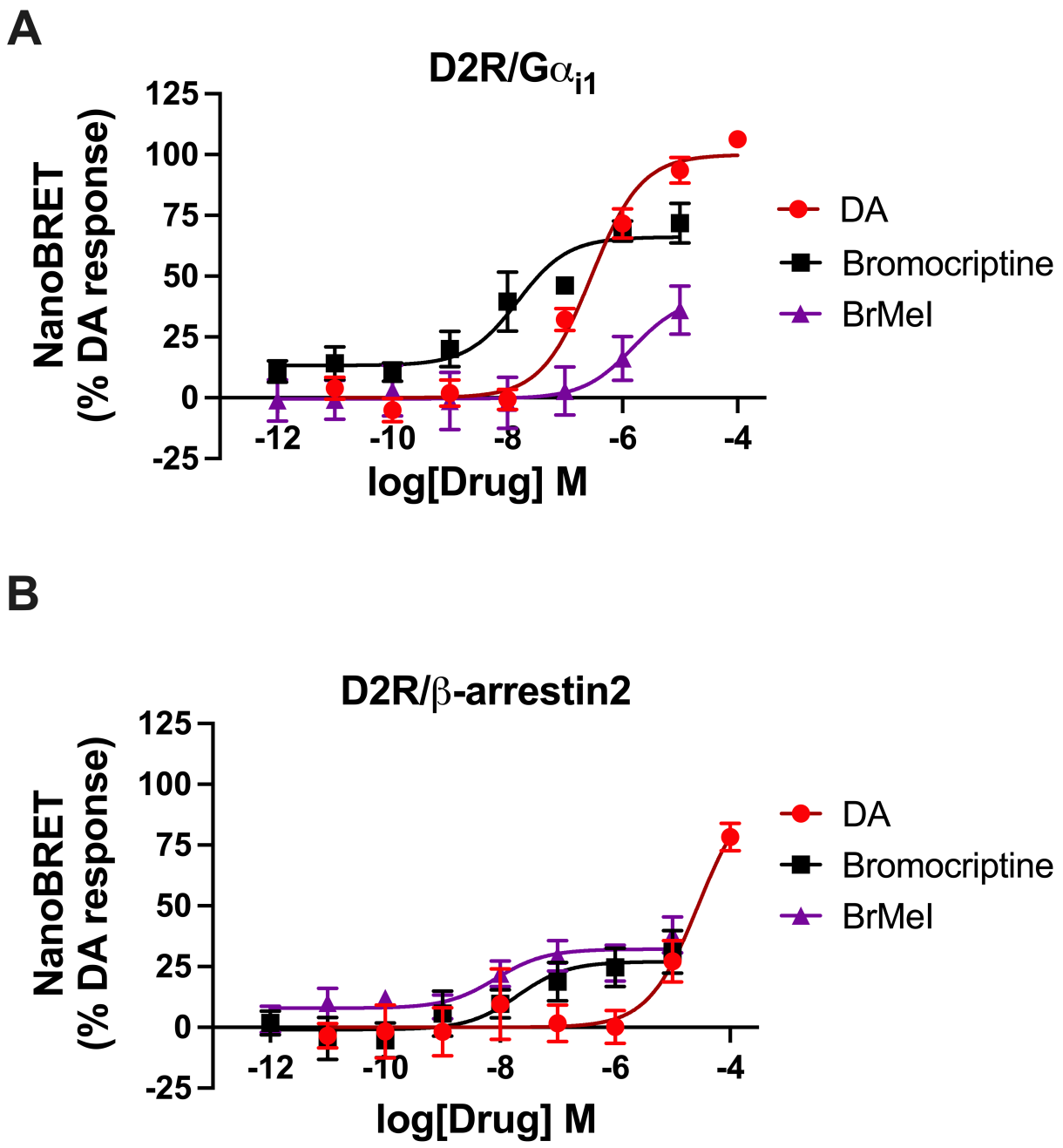

Figure 4. Bromocriptine methiodide stimulation causes preferential recruitment of β-arrestin2 to D2R. Concentration-response nanoBRET assays examining recruitment of G protein $G\alpha_{i1}$ and β-arrestin2 to D2R in response to stimulation by DA (red circle), unmodified bromocriptine (black square), or bromocriptine methiodide (BrMeI, purple triangle). HEK-293T cells expressed HaloTag-labeled D2R and either NanoLuc-labeled $G\alpha_{i1}$ or β-arrestin2 as the

respective nanoBRET pairs. **(A)** Stimulation by DA, bromocriptine, or BrMeI resulted in dose-dependent $G\alpha_{i1}$ recruitment to D2R. BrMeI was less efficacious or potent (EC_{50} = 1.52 μM) than either canonical D2R ligand DA (EC_{50}=0.29 μM) or bromocriptine (EC_{50} = 15.07 nM). **(B)** BrMeI was more potent in eliciting β-arrestin2 recruitment to D2R (EC_{50} = 8.37 nM) compared to bromocriptine (EC_{50} = 20.13 nM) or DA (EC_{50} = 27.63 μM). BrMeI exhibited β-arrestin2 recruitment efficacy similar to bromocriptine but was 4-fold less efficacious than DA. NanoBRET data were baseline-corrected and normalized to % maximal DA response. Assays were performed in triplicate from n ≥ 3 independent experiments. Data are represented as mean ± SEM for all experimental replicates.

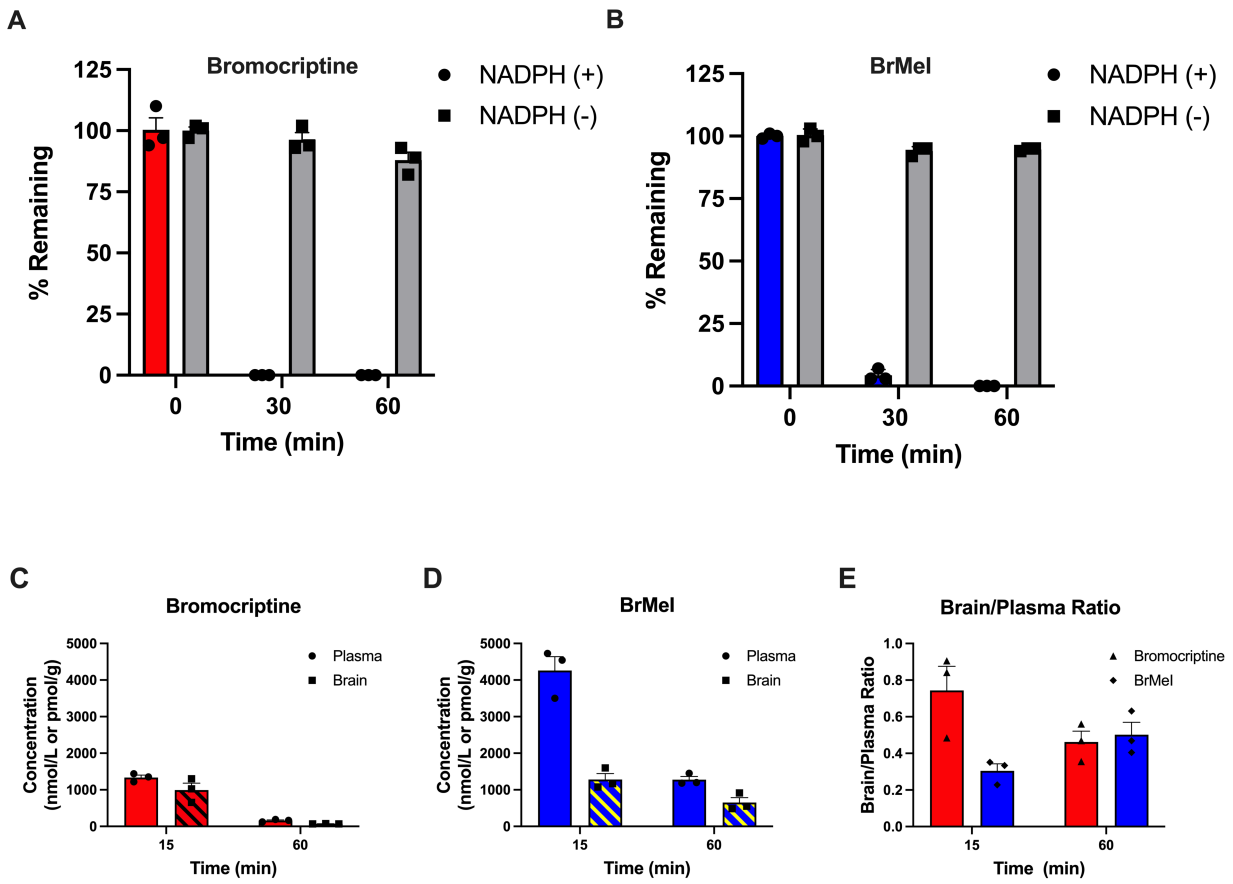

Figure 5. Phase I metabolic stability and pharmacokinetic analysis of BrMel versus bromocriptine. (A, B) Phase I metabolic stability assay of BrMel versus bromocriptine. BrMel and bromocriptine (1 μM) were incubated with mouse liver microsomes in the presence or absence of NADPH (negative control). % drug remaining across time was measured by LC/MS/MS. Bromocriptine **(A)** and BrMel **(B)** underwent significant Phase I metabolism in mouse liver microsomes. Bromocriptine was entirely metabolized within 30 min. For BrMel, <5% of the drug similarly remained by 30 min and 0% within 60 min. Data are represented as the mean % remaining drug ± SEM (n = 3 per time point). **(C-E)** Pharmacokinetic analysis of BrMel versus bromocriptine in mice. Brain and plasma concentrations of BrMel and bromocriptine were measured at 15 min and 60 min following intravenous administration (10 mg/kg for both drugs). Bromocriptine **(C)** exhibited lower plasma levels at both time points compared to BrMel **(D)**. Plasma levels of BrMel remained 8-fold higher at 1 h compared to bromocriptine. **(E)** The brain-

to-plasma ratios for BrMeI were lower at 15 min but similar at 60 min. Data are represented as the mean ± SEM (n=3 per group).

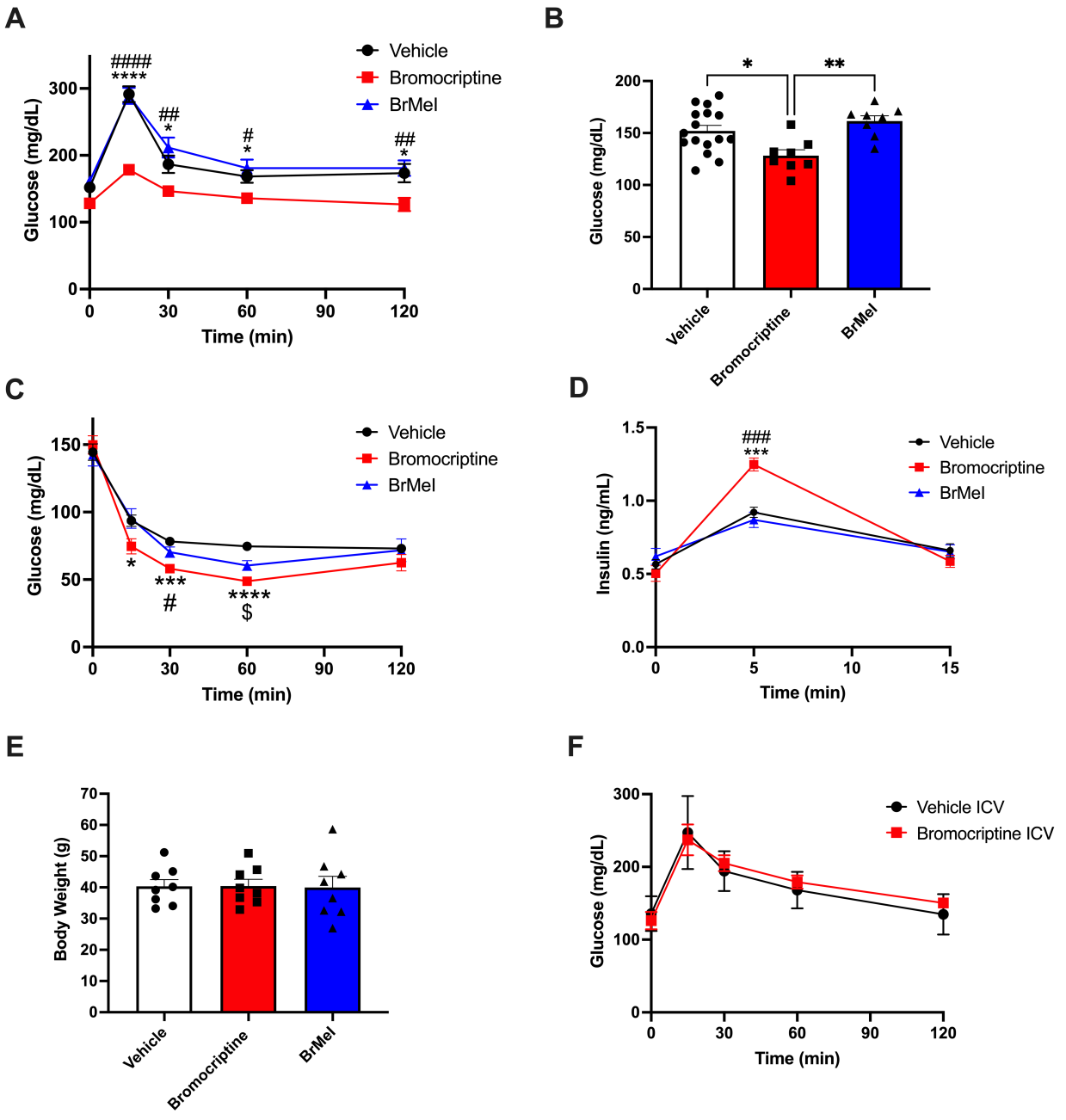

Figure 6. Tandem targeting of central and peripheral dopaminergic targets is required for treating dysglycemia *in vivo*. (A) Western diet-fed dysglycemic mice were systemically treated with bromocriptine (10 mg/kg i.p., in red), BrMel (10 mg/kg i.p., in blue), or vehicle (i.p., in black). Oral glucose tolerance testing (OGTT, 2g/kg glucose) revealed significant effects of drug treatment ($p < 0.0001$) on improvement in glucose tolerance driven by bromocriptine ($n = 8$); BrMel ($n = 8$) did not significantly modify glucose tolerance ($p > 0.05$) versus vehicle ($n = 16$).

*<0.05 bromocriptine versus vehicle; #<0.05, ##<0.01, ####<0.0001 bromocriptine versus BrMeI. **(B)** Bromocriptine-treated mice (n = 8) exhibited significantly lower fasting blood glucose compared to BrMeI (p = 0.0035, n = 8) or vehicle (p = 0.0163, n = 16). *<0.05, **<0.01. **(C)** Insulin tolerance testing (ITT) showed that bromocriptine treatment (10 mg/kg i.p., in red; n = 8) led to significant improvements in insulin sensitivity versus vehicle (i.p., n = 8), with smaller improvements produced by BrMeI (10 mg/kg i.p., n = 8). *<0.05, ***<0.001, ****<0.0001 bromocriptine versus vehicle; #<0.05 bromocriptine versus BrMeI; $<0.05 BrMeI versus vehicle. **(D)** Bromocriptine treatment also significantly enhanced plasma insulin levels during the ITT compared to BrMeI (p = 0.0003) or vehicle (p = 0.0002) groups. ***<0.001 bromocriptine versus vehicle, ###<0.001 bromocriptine versus BrMeI. **(E)** There was no significant effect of bromocriptine or BrMeI on body weight versus vehicle treatment in Western diet-fed wild-type mice (p > 0.05) (n=8/group). **(F)** I.c.v. administration of bromocriptine (10 mg/kg, in red) in Western diet-fed dysglycemic wild-type mice. OGTT (2 g/kg glucose) did not significantly modify glucose tolerance versus i.c.v. vehicle treatment (in black) (n=8/group; p>0.05). All data represented as mean ± SEM.

Compound	D2R	D3R	D3R/D2R
	K_i ± SEM (nM)	K_i ± SEM (nM)	
(-)-Quinpirole[a]	13.1 ± 2.2	6.76 ± 1.2	0.52
AB01-59	141.0 ± 52.4	459.0 ± 80.5	3.26
Bromocriptine	0.59 ± 0.17	2.05 ± 0.56	3.46
AB01-60	3.14 ± 0.34	17.50 ± 4.90	5.57
Sumanirole[a]	46.3 ± 2.6	573 ± 118	12.38
MPE01-05	129.0 ± 20.5	1840 ± 271	14.26
(±)-7-OH-DPAT	5.09 ± 1.21	3.42 ± 0.72	0.67
AB01-62	912 ± 117	1250 ± 183	1.37
(+)-PD128,907	18.8 ± 4.7	2.65 ± 0.14	0.14
AB01-117	94.1 ± 20.5	18.7 ± 4.3	0.20
CAB03-015	140.0 ± 39.6	806 ± 145	5.76
AB01-102	1750 ± 276	2900 ± 456	1.66
Aripiprazole[a]	0.48 ± 0.05	3.57 ± 0.79	7.44
AB01-61	437 ± 60	1970 ± 360	4.51
L741,626	8.47 ± 0.99	54.1 ± 13.0	6.39
MPE01-06	1660 ± 327	1130 ± 440	0.68

Table 1. Radioligand competition D_2-like receptor binding data. Equilibrium dissociation constants (K_i) indicate human D2R and D3R binding affinities for dopamine D_2-like receptor-selective drugs and their respective quaternary MeI analogues. The ratio of D3R/D2R binding affinity was calculated alongside each compound. All compounds were tested with [^{3}H]-(R)-(+)-7-OH-DPAT, except for L741,626 and MPE01-06 which employed [^{3}H]N-methylspiperone. K_i values are represented as mean ± SEM with n ≥ 3 independent experiments performed in triplicate. [a]Data previously reported in Bonifazi et al. (2017).

Compound	D2R		D3R	
	EC_{50} ± SEM (nM)	E_{max}	EC_{50} ± SEM (nM)	E_{max}
(-)-Quinpirole	35.8 ± 5.8	102%	3.9 ± 1.0	102%
AB01-59	890 ± 190	109%	56 ± 14	124%
Bromocriptine	0.63 ± 0.21	99%	3.4 ± 1.1	116%
AB01-60	9.8 ± 2.9	88%	38 ± 11	91%
Sumanirole	164 ± 54	110%	224 ± 24	180%
MPE01-05	472 ± 79	105%	386 ± 76	172%
(±)-7-OH-DPAT	10.8 ± 1.6	106%	0.54 ± 0.17	97%
AB01-62	3520 ± 610	105%	598 ± 58	102%
(+)-PD128,907	ND		0.78 ± 0.28	98%
AB01-117	ND		47 ± 14	98%
CAB03-015	ND		>10000 (IC_{50} = 2770 ± 310)	<1% (I_{max} = 83%)
AB01-102	ND		>8300 (IC_{50} = >8500)	6% (I_{max} = 64%)
Aripiprazole	3.8 ± 1.5	25%	18.3 ± 5.6	29%
AB01-61	6100 ± 1300	29%	1660 ± 670	27%
L741,626	>10000	<1%	>10000	<5%
MPE01-06	>10000	<0%	>10000	<2%

Table 2. Functional activity in D2R- and D3R-mediated mitogenesis assays. EC_{50} and E_{max} values were calculated from dose-response curves of drug-stimulated mitogenesis in CHO cells expressing either human D2R or D3R. EC_{50} values are represented as the mean ± SEM. E_{max} values represent % maximal efficacy relative to quinpirole stimulation. Data are from n ≥ 3 independent experiments performed in triplicate. ND, not determined.

Compound	pIC_{50} (IC_{50}, μM)	E_{max}
(-)-Quinpirole	5.93 (1.18)	100.00%
AB01-59	5.16 (6.94)	51.56%
Bromocriptine	6.75 (0.18)	166.94%
AB01-60	4.99 (10.17)	190.02%
Sumanirole	3.75 (17.92)	171.44%
MPE01-05	3.73 (18.50)	171.44%
(+)-PD128,907	4.34 (45.43)	195.52%
AB01-117	4.01 (98.19)	166.63%

Table 3. Drug potencies and efficacies on glucose-stimulated insulin secretion (GSIS). Potency data are represented by pIC_{50} with corresponding IC_{50} values in parentheses (in μM). E_{max} values represent % maximal efficacy relative to (-)-quinpirole treatment.

Drug	Time (min)	Plasma Conc. (nmol/L)	Brain Conc. (pmol/g)	Brain/Plasma Ratio
Bromocriptine	15 min	1336.7 ± 52.2	995.2 ± 188.0	0.74 ± 0.11
	60 min	158.6 ± 15.0	71.1 ± 2.3	0.45 ± 0.05
BrMel	15 min	4259.1 ± 381.3	1282.3 ± 130.7	0.30 ± 0.03
	60 min	1277.1 ± 71.1	651.9 ± 133.7	0.51 ± 0.06

Table 4. Quantification of *in vivo* pharmacokinetics of BrMel versus bromocriptine in mice.

Data are represented as the mean ± SEM (n=3 per group).